Rockfall Hazard Assessment: An Overview

15

Biswajeet Pradhan and Ali Mutar Fanos

15.1 Introduction

Rockfalls are landslides that exhibit mass movements and highly varied volume and that involve rock masses ranging from several cubic centimeters to thousands of cubic meters. Rockfalls happen when rock masses are detached from a cliff face and freely fall under the effect of gravity (Blahut et al. 2013; Youssef et al. 2015; Varnes 1984). Even small-magnitude events can be extremely destructive because of their high velocities reaching up to tens of meters per second; they can potentially damage roads and cause fatalities. After a landslide occurs, rockfalls are among the natural hazards that mostly affect roads with steep roadside cuttings through brittle rock masses (Kharel and Dhakal 2013). Therefore, a rockfall is a serious natural disaster in mountainous regions and poses a major threat to infrastructure, transportation networks, and people.

Rockfalls are composed of detached rocks from a cliff face, with subsequent free-falling (flying), bouncing, sliding, and rolling motions along a slope surface with high velocity (Arbanas et al. 2012; Ferrari et al. 2013; Leine et al. 2014). Rock detachment is basically attributed to discontinuities, as well as to relevant weathering and deterioration, along surfaces. Major triggering factors of rockfalls include saturation, erosion, freezing temperatures, weakening caused by water runoff, earthquakes, wildfires, the presence of vegetation roots, frequent freeze–thaw cycles, thermal expansion–contraction, and high rainfalls (Asteriou et al. 2012; Wyllie 2014; Sabatakakis et al. 2015).

Traditional surveying techniques restrict the gathering of spatial datasets to generate digital elevation models (DEMs) required for rockfall modeling (Salvini et al. 2013). In the last decade, new remote sensing technologies and powerful geographical information systems (GIS) have increased topographic information, thereby providing a basis for developing new methodologies to analyze Earth surfaces; moreover, new techniques, such as light detection and ranging (LiDAR), have risen rapidly in the fields of geohazard assessment and modeling. At present, both airborne and ground-based LiDAR surveys are essential for analyzing detailed topographies (Fanos et al. 2016; Youssef et al. 2015; Barbarella et al. 2013; Pradhan et al. 2005; Tonini and Abellan 2014; Stephenne et al. 2014; Fanos and Pradhan 2016).

15.2 Slope Failure Problem

Rockfalls pose considerable threats to public transportation networks and properties located in hilly regions and rock cuttings. However, rockfalls are not as economically dangerous as large-scale failures that can block vital roads for days. Rockfall fatalities tend to be of the same order as those in other types of rock slope instabilities. Martin (1988) reported that rockfalls, small rockslides, and ravelings are the most frequent problems on road transportation networks in the mountainous regions of North America. Hungr and Evans (1988) reported 13 rockfall fatalities in the last 87 years in the mountain motorways of British Columbia, Canada. Over the last decades, increasing incidents of slope failure has been observed in Malaysia. Most of these incidents have occurred on cut slopes or embankments alongside roads and highways in mountainous areas (Pradhan et al. 2010). Shu and Lai (1980) recorded a major rockfall event in Gunung Cheroh, Ipoh, Malaysia. This event involved the collapse of the entire face of a cliff as a single plate weighing approximately 23,000 tons and measuring 33 m in length. It resulted in 40 fatalities, and numerous cattle were also killed. Among the most recent disastrous slope failures occurred on August 7, 2011, in Kampung Sungai Ruil, the Cameron Highlands. Another incident occurred on May 21, 2011, in Hulu Langat. Moreover, a rockfall buried the back portion of

B. Pradhan (✉) · A.M. Fanos
Department of Civil Engineering, University Putra Malaysia, Serdang, Malaysia
e-mail: biswajeet24@gmail.com

B. Pradhan (ed.), *Laser Scanning Applications in Landslide Assessment*,
DOI 10.1007/978-3-319-55342-9_15

an illegal factory located at the foothills of a limestone hill in Bercham, Ipoh, Perak, western Malaysia in December 2004. This incident caused two deaths. Some rockfall incidents have not resulted in fatalities but have caused major inconveniences. Examples include the Athenaeum Condominium in Ulu Kelang in May 1999 and the rocky slope failure in Bukit Lanjan on the New Klang Valley Expressway in 2003. Both events resulted in traffic disruptions that lasted for six months.

15.3 Rockfall

A "rockfall" is a slope process that involves rock fragment detachment and their subsequent falling, bouncing, rolling, sliding, and deposition (Varnes 1978). In certain cases, rockfalls are quantitatively measured by describing the insignificant phenomenon of falling blocks of rocks of a few cubic meters up to 10,000 m^3. Meanwhile, "rockslides" are characterized by falling blocks of over 100,000 m^3, whereas "rock avalanches" may extend to a few million cubic meters (Dussauge-Peisser et al. 2002). Rockfalls occur regularly when one or multiple blocks fall, bounce, slide, or roll down a slope. In a scree slope, a falling block may move beyond the slope edge and stop at a certain distance from the base of the slope. Falling blocks pose the largest hazard to the surrounding areas of a slope, and their uncertain behavior is a major challenge in assessing rockfall hazards (Evans and Hungr 1993).

15.4 Rockfall Definitions

"Rockfalls" or "rockfalls" refer to rock quantities that fall freely from a cliff face. Rockfalls are rock fragments (blocks) that detached by sliding, falling, or toppling, and then fall off a steep cliff face (vertically or a sub-vertically), moving downslope by flying, bouncing over ballistic trajectories, or rolling over talus or debris slopes (Varnes 1978). Chen et al. (1994) defined a "rockfall" as a sudden independent block movement or a complex of continuous rock detachments from a steep slope. Lee and Elliot (1998) defined "rockfall" as "the downslope boulders movement (from natural slopes) or blocks (from cut faces) which, when not correctly restrained, have the potential to damage or destroy structures along their trajectory or creating an impediment to the public transportation networks."

Richards (1988) provided a summary of commonly accepted properties of rockfalls as follows:

- A rockfall event comprises one block or a set of blocks that detached from a cliff face.
- Each falling rock behaves independently of other rocks.
- A temporary loss of earth contact and high downhill acceleration occur.
- Blocks gain significant kinetic energy during their descent.

Rockfall failures vary from slipping failures that form on the slipping surface of rocky slopes. Rockfalls, which include small individual rock blocks, should be differentiated from rock avalanches, which is characterized by a huge amount of mass motion and a portion of the entire slope (which can include the bed rock and the slope face) collapsing suddenly.

15.5 Methods of Data Collection for Rockfall Hazard Analysis

The essential variables of rockfall hazard analysis are shown in Fig. 15.1. Susceptibility, magnitude, rockfall run-out, and exposure are frequently assessed using well-set mapping and measurement methods or directly defined by in situ specialists using a heuristic approach. Current developments in digital data collection platforms and widely available computing resources have allowed digital and indirect assessments of rock mass stability. Such remote sensing techniques involve LiDAR and photogrammetry.

15.5.1 Heuristic or Experience-Based Approaches

The heuristic or experience-based approach is frequently used for rock mass assessment when rock assessment experts are available, and failure modes and geological settings are well understood by the experts. Mining environments depend heavily on heuristic assessment because in situ experts are regularly exposed to geological, structural, and failure models. Nevertheless, in spatially different circumstances, such as transportation corridors where complicated and varying geologies and failure modes can be estimated, heuristic approaches are only utilized at the primary level to identify rock masses that require further assessment and possible mitigation techniques (Ruff and Czurda 2008).

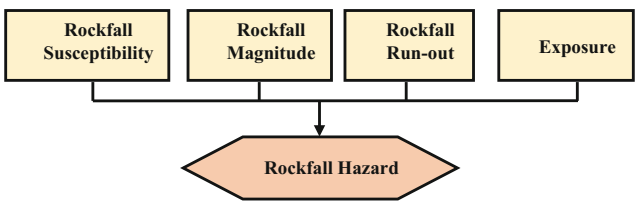

Fig. 15.1 Rockfall hazard evaluation framework

15.5.2 Mapping and Measurement Techniques

Mapping and measurement methods include the immediate physical exposure of the assessing engineer to a possibly unstable rock mass. The engineer typically measures visibly accessible structural characteristics, such as discontinuities involving joints, beds, and faults. The engineer will also assess positional parameters, such as physical setting (height, slope length, and face angle), and how a rock mass interacts with a highway in man-made/natural obstacles (e.g., barriers) and the presence of shoulders and ditches. These measurements and geologic mapping results form the bases for a rockfall hazard evaluation system (Crosta and Agliardi 2004).

15.5.3 Photogrammetric Analysis

Photogrammetry methods for the rock mass assessment of potentially unstable slopes include the alignment and 3D projection of two stereo photographs. The output 3D stereo photographs enable the assessment of rock mass geometry and structure. Discontinuity orientation is measured, faults are detected, and kinematic instability is computed. Photogrammetry methods for rock mass assessment are widely published and adopted in the geological community. Comprehensive examples of processing and data collection techniques are provided in Kemeny and Post (2003) and Haneberg (2007).

15.5.4 Light Detection and Ranging (LiDAR)

LiDAR is a range-based imagery technique that can create an accurate 3D model of the Earth surface within a short period. LiDAR data are basically gathered via mobile aerial surveying (e.g., using helicopters and airplanes) or static terrestrial (using a tripod) methods. The resulting datasets include millions to billions of points in a space coordinate (XYZ) that can be converted into geographical coordinates, such as the Universal Transverse Mercator (UTM). Every point information group typically includes a "color" value associated with the measured intensity of a returning beam as detected by a scanner or associated with the true colors derived from a combination of photographic techniques (Höfle and Rutzinger 2011).

Remote geomechanical assessment of structural discontinuity has conventionally involved the use of photogrammetry techniques. In recent years, technological advancements have led to the assessment and use of LiDAR-based techniques in remote geomechanical analyses. Discontinuity mapping accuracy using LiDAR data should be assessed and compared with conventional compass-based methods prior to implementing LiDAR in engineering workflows (James et al. 2007).

15.6 Rockfall Research Background

Initial research on rockfall behavior was conducted by Ritchie (1963). He stated the necessity for a prediction method for the material stability of rock cut surfaces. Moreover, he developed standards for designing ditches and cut slopes (Fig. 15.2) by performing hundreds of full-scale rockfall tests. These tests are still extensively used in rockfall protection design at present. Ritchie (1963) investigated the movements and trajectory of rocks and attempted to formulate an analytical solution for rockfall based on movement laws.

Subsequent to Ritchie's work, substantial progress has been achieved in rockfall behavior analysis. Most of these studies are relevant to the highway projects. Rockfall research has been conducted by empirical investigations, physical simulation, and computer simulation (Dorren 2003). Initial research was typically accomplished via empirical approaches, whereas computer modeling has been widely used in the past two decades.

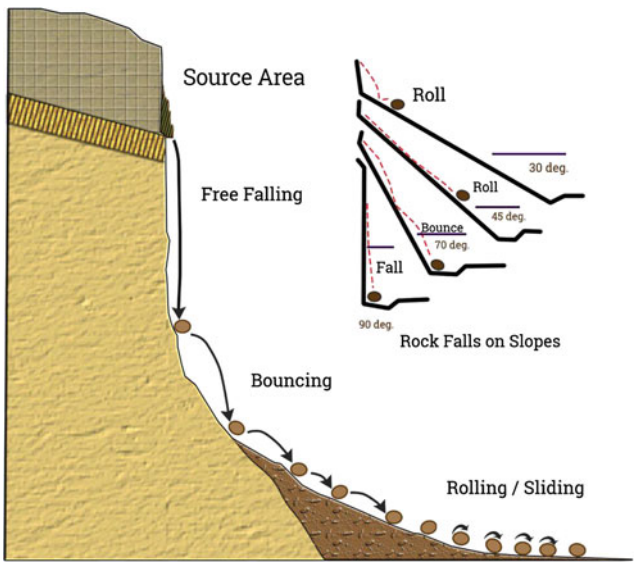

Fig. 15.2 A typical rockfall process and the rockfall design standards based on Ritchie's (1963) work

15.7 Rockfall Mechanics

Ritchie (1963) provided design criteria for describing relationships among the variables of cliffs, namely slope angle, ditch depth, and fallout area width. Rockfall mechanics for cliffs and slopes have been considered to propose different solutions, including fences or barriers and ditches to accommodate rockfalls. With regard to problematic slope gradients, Ritchie (1963) noted that a large rock had a long run-out distance from the origin. He observed that a falling rock would spend more time in the air and would stop when the slope became sufficiently flat and slope irregularity became sufficiently high to reduce rock velocity. Ritchie also proposed a mechanical approach to describe rockfall trajectory. He explained rock path as a sequence of parabolic trajectories affected by the impact angle that determined the velocity along and perpendicular to the effect plane. Ritchie also suggested that the shape and size of a rock have minimal effect on its falling or rolling characteristics. He inferred that a falling rock must follow particular laws of energy, mass, restitution, velocity, and impact, although it would be affected by friction, time, and gravity. The mechanical considerations of Ritchie are associated with a single rock and its movement is unaffected by neighboring rock fragments involved in a rockfall. Potential energy due to gravity is transformed into kinetic energy in rockfalls. The line that connects the rockfall origin and the final deposition of the rockfall is known as the "energy line," and the gradient is known as the "energy line angle" (Salvini et al. 2013).

15.8 Rockfall-Triggering Factors

Rockfalls begin with the detachment of rocks from a cliff face in a rockfall source region (Youssef et al. 2015). Rocky slopes are subjected to varying weathering degrees that can cause joint opening and cracking, thereby promoting rockfall. Rockfall promotion degree relies on the elements of the environment that cause weathering, i.e., chemical and physical, and on bedrock type (Day 1997). The triggering mechanism determines the occurrence of a rockfall regardless of the weathering rate. The triggering factors of rockfall conditions and mechanisms have been widely characterized in the literature. Rockfall-triggering mechanisms can be classified into rockfall motivators and movement causes. Nevertheless, differentiating between movement causes and rockfall motivators is complicated because a particular process, such as frost shattering, typically motivates weathering that leads to rockfall. Moreover, slope morphology and the direct neighborhood of probable falling rocks are significant elements for determining whether rocks will fall.

Gardner (1983) observed rockfalls in a mountainous region and concluded that such phenomena occurred particularly on glaciers over steep rocky slopes that were alternately subjected to thawing and freezing. Such rockfalls occur frequently, have small magnitudes, and are common in steep regions (Jomelli and Francou 2000). Similarly, Douglas (1980) examined frequent and small-magnitude rockfall events and proved that such events were caused by frost. Nevertheless, he declared that the geotechnical characteristics of the bedrock play a significant role. These findings corroborated the opinion of Luckman (1976), who demonstrated that the geological and morphological natures of cliffs and the variations in temperature of rock surfaces controlled rockfalls. Vidrih et al. (2001) characterized different rockfall causes and explored the correlation between earthquake activities and rockfalls. They inferred that earthquakes would trigger rockfalls. Wieczorek et al. (2000) reported that rockfalls could be triggered by various causes, such as seismic activities, water freezing–thawing cycles in joints, rapid snow thawing, rainstorms, root wedging and permeation, and stress relief deglaciation. In most studies on slope movements, factors that triggered the movements were either unnoticed or unreported. Reported rockfall events have indicated that the rapid melting of snow, earthquakes, and extensive winter rainstorms have caused more movements than human activities and freezing–thawing conditions. Human activities that reduce slope stability in hard rocks remain the main element compared with geological elements, but may vary significantly, such as in the undercutting of slopes through excavations or quarrying for infrastructure. Moreover, animals can also cause rockfalls, such as goats climbing on steep rock faces.

The overall view demonstrates that diverse elements have been recorded as rockfall-triggering parameters. In most cases, however, geological, topographical, and climatic factors combined with time determine whether a rockfall will occur. A dynamic analysis by Salvini et al. (2013) concluded that water saturation and the implemented acceleration of earthquakes could affect the stability of nearly all blocks. A gradual decrease in the stability of steep rocky slopes is one of the potential effects of warming in high mountain areas. Lately, the possible direct role of warm temperatures in triggering rockfalls has been studied (Allen and Huggel 2013). Rockfalls in Malaysia are mainly triggered by tropical rainfall and flash floods that cause failure of the rock surface along fractures, joints, and cleavage planes (Pradhan 2010; Pradhan and Lee 2010).

15.9 Motion Modes of Falling Rocks

After a rock detaches and proceeds downslope, it descends the slope in various motion types. The type of movement highly depends on the mean of the slope incline (Fig. 15.3). The most significant motion modes are free-falling or flying through the air, bouncing over the surface of a slope, and sliding or rolling on the slope surface.

15.9.1 Free-Falling of Rocks

The free-falling of rocks occurs when slopes are extremely steep. Ritchie (1963) stated that the free-falling of rocks would occur if the gradient of the slope was greater than 76°. However, this value varies in different field conditions. Figure 15.1 illustrates that rock movements of approximately 70° transform gradually from bounce to fall.

Azzoni et al. (1995) mentioned that two types of movements could occur during the free-falling of rocks. The first movement is the translation of the rock center, whereas the second is the rotation of the block around the center. Rotation and translation are significant because falling blocks are never round in shape. After a rock rotates in the air, it can bounce in various directions following impact compared with its previous direction. The velocity of a free-falling rock is affected by air friction. Nevertheless, Bozzolo and Pamini (1986) noted that air friction would not affect rock movement. Azzoni et al. (1995) reported that a rock colliding with other falling rocks also influenced free-falling rocks and their trajectories. However, this effect is difficult to analyze during rockfall events or field surveys.

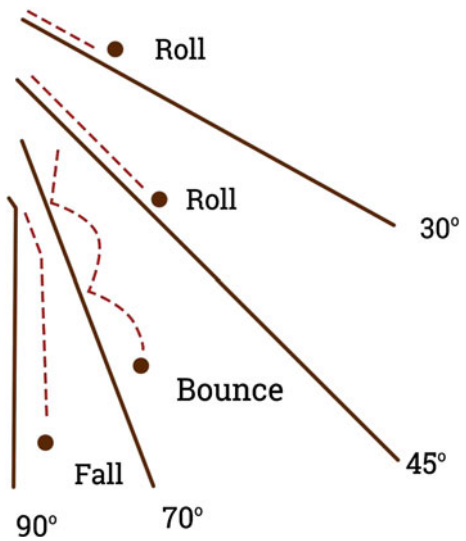

Fig. 15.3 Motion modes of rock during their fall on slopes based on the mean gradients of slope (Ritchie 1963)

15.9.2 Bouncing, Rolling, and Sliding of Rocks

Rock movement occurs on or close to the surface of a slope when the mean incline of the slope is reduced in the downslope section. After free-falling, a rock collides with the surface of the slope; this movement is defined as rock bouncing. Rocks, particularly weak ones, tend to break down into fragments at first bounce (Bozzolo and Pamini 1986). Evans and Hungr (1993) stated that 75–85% of the energy from the first fall was lost during the first collision regardless of whether a rock broke or not. When the mean gradient of the slope is lower than approximately 45°, rock movement transforms gradually from bouncing to rolling because of the rotational momentum collected by the rock. Moreover, a rolling rock is nearly permanently in touch with the surface of a slope (Hungr and Evans 1988). During the transition from bouncing to rolling, a rock revolves rapidly and only the edges with a high radius come in contact with the slope surface. Thus, the center of gravity moves along a nearly direct path, which is an effective movement mode with regard to energy loss. Erismann (1986) stated that the combination of bouncing and rolling was among the major mechanisms of displacement. Sliding is another type of movement on a slope surface. However, sliding typically occurs only during the first and final phases of a rockfall event. As a sliding rock begins to fall, it bounces or rolls as the mean incline of a slope increases. A rock normally stops because of energy loss due to friction if the mean gradient of a slope does not change during sliding (Bozzolo and Pamini 1986). Basson (2012) reported that a falling rock could exhibit four types of movement along its track: free-falling, rolling, bouncing, and sliding. Typically, a rockfall incident experiences more than one of these movements. During free-falling, no interaction occurs between the slope and the falling body; however, an interaction occurs for the other types of motion, during which the rock can be fractured into smaller portions.

15.10 Lateness of Moving Rocks

A moving rock stops after experiencing various modes of motion. The velocity and stopping of a falling rock rely primarily on the mean incline of a slope because a falling rock normally decelerates on a flat slope and accelerates on a steep slope. In addition to the mean incline of the slope, velocity depends on the material that covers the slope, such

as soil, vegetation, and scree. Small rocks are easier to stop than large ones because their kinetic energy that aggregates during a rockfall is less than that of the large rocks. Small rocks can be easily stopped by huge obstacles, such as trees. Moreover, they can be easily impeded in the depressions among larger boulders on a slope surface. These reasons are the major sorting effects on falling rocks over a slope (Statham and Francis 1986). In general, the sorting effect should only be considered for the upper portion of scree slopes because rocks with varying sizes in avalanches are mainly deposited at the base (Jomelli and Francou 2000). The stopping of falling rocks is a gradual process rather than a sudden one. Rocks stop because of energy loss from collision forces and friction along the surface of the slope. The frictional force of moving rocks does not only depend on their shape, but also on the characteristics of the slope surface (Statham and Francis 1986). These characteristics can vary considerably within short distances. Thus, the frictional force between the slope surface and a rock can be described using the dynamic angle of friction. The dynamic angle of friction is associated with surface roughness, which has been defined by Pfeiffer and Bowen (1989) as the height variation perpendicular to the slope within a particular distance of the slope. The dynamic angle of friction of falling rocks is described by Kirkby and Statham (1975) as shown in Eq. (15.1):

$$\tan \phi_{ud} = \tan \phi_0 + c * d(2 * r) \qquad (15.1)$$

where ϕ_{ud} is the friction dynamic angle (°); ϕ_0 is the internal friction angle (°), which ranges from 20.3° to 33.7°; c is a constant ranging from 0.16 to 0.25; d is the mean scree diameter on the surface of the slope (m); and r is the rock radius (m).

Forest cover also affects the transportation of scree or large rocks. Zinggeler et al. (1991) studied the significance of trees in stopping falling boulders and inferred that the topography of a slope surface was equally significant; moreover, the collision of falling rocks with tree trunks led to energy loss, thereby ultimately causing rocks to stop in flat regions of a slope surface. Hétu and Gray (2000) noted the influence of a forest on scree movement on a slope surface. They observed that the concentration of rocks over forest edges on scree slopes increased with increasing forest density. Moreover, they mentioned the permanent struggle between forest settlement and active scree slope development. The front area of an active scree slope moves downslope when a forest is disrupted by fire or a large-scale mass movement. Their research elucidated the incapability of forests to stop large-scale destruction from rockfall incidents; however, forests provide efficient protection for small-scale and high-frequency rockfall events.

15.11 Rockfall Modeling and Analysis

Several models can calculate run-out areas of rockfall incidents and their characteristics in terms of trajectory, frequency, velocity, bouncing height, and kinetic energy (Volkwein et al. 2011). All existing rockfall models can be divided into three major types: (1) process-based, (2) empirical, and (3) GIS-based rockfall models.

15.11.1 Process-Based Rockfall Models

Process-based models simulate or explain rockfall movement modes over slope surfaces. Gigli et al. (2014) used 2D and 3D rockfall simulation models to calculate bounce height, rock velocity, and kinetic energy based on rock position along the profiles or on the slope. A 3D rockfall model was utilized to simulate the effect of slope morphology on rockfall trajectories at the regional scale, whereas a 2D rockfall model enabled implementation of a larger number of simulations along the slope profiles specified by the 3D modeling. The lumped mass approach was applied in the two models. Each rock was symbolized by a simple point with its mass settled at the center, and rockfall trajectories were simulated by considering the physical laws that controlled the sequence of various rockfall motion modes (free-falling or flying, bouncing, rolling, and sliding). As an effective and rational technique for protection measures and performance-based design, a 3D rockfall simulation technique assists in depicting rockfall motion on a slope and in probabilistically considering vegetation impact.

Masuya et al. (2009) elaborated a typical evaluation technique and analyzed the manner in which a rockfall combined with vegetation interference and other elements. As an application, a real slope where a rockfall occurred because of an earthquake activity was examined. The advantages and validity of the proposed technique were used as bases for the measurement planning and hazard mapping of a rockfall. Ma et al. (2011) simulated actual rockfall via discontinuous deformation analysis. In the simulation, rockfall energy losses were classified into three types: friction loss, collision loss, and loss by vegetation. The result of the in situ experiments illustrated that energy loss resulting from collision was among the most significant elements. Rockfall impact force is defined by its movement velocity and behavior, which are conditioned by slope incline, rock shape, height, and surface roughness of the rockfall trajectory.

Undulating and rough slopes tend to cause changes in rockfall trajectories. An irregular slope easily changes the behavior of a rockfall movement from sliding or rolling to bouncing. Moreover, a large slope incline increases bounc-

ing movement behavior, whereas a small slope incline easily initiates sliding and rolling. Furthermore, slope surface undulation immediately influences rock collision angle, and rockfall behavior easily changes from sliding or rolling modes to bouncing mode (Wang and Lee 2012).

15.11.2 Empirical Rockfall Models

Empirical rockfall models are typically based on the correlation between the topographical factors and trajectory length of rockfall incidents. Such models are occasionally defined as statistical models (Keylock and Domaas 1999). Leine et al. (2013) developed a complete 3D simulation method for rockfall dynamics. The simulation of a rockfall was performed using hard contact laws based on the non-smooth contact dynamic technique. The rock was modeled similar to that of an arbitrarily convex polyhedron, and the terrain was modeled using a high-resolution DEM. Leine et al. (2013) proposed a specialized law of friction for rockfall that provided scarring behavior description (i.e., a falling rock tended to slide before bouncing on a slope surface). The geometry of rock effect on rockfall dynamic has been examined using two numerical simulations. Topal et al. (2007) devised a 2D rockfall assessment that was performed over several slope profiles. Rockfall characteristics in terms of run-out distance, bouncing height, kinetic energy, and rock velocity over each profile were evaluated using the 2D rockfall model. The outcomes of the simulation were utilized to outline the regions at risk. Mikoš et al. (2006) used a 2D rockfall simulation program to analyze rockfall in two longitudinal profiles. First, the program was calibrated in a previous rockfall event in two longitudinal profiles using different numbers of blocks. The initial values of the associated model parameters were obtained from the literature, and various combinations were tested.

Rockfall run-out has been largely determined based on terrain roughness and surface characteristics. The number of released blocks affects run-out distance. In particular, when the roughness of a slope surface is high, a relatively large number of released blocks should be used. Large blocks have a larger bounce height and higher total kinetic energy but lower run-out distance than small blocks. A forest may virtually stop blocks that are less than 0.2 m, but has no effect on 6 m blocks. The calibrated model has been applied to another rockfall event in two longitudinal profiles without and with a gallery for rockfalls. The results of the simulation (bounce height, total kinetic energy) confirmed the appropriateness of the gallery location. They concluded that silent witnesses, such as released blocks and tree damages, should be used in the case of an active rockfall; otherwise, more than one profile should be simulated. They also mentioned that the upper scar on the rock face should be considered in the calculation. In the case of active rockfalls, rock face color indicates the release points. Silent witnesses may help to a certain extent. Therefore, a rockfall model should be calibrated with another rockfall event under same the field conditions before it can be used.

Ahmad et al. (2013) studied various numerical simulations using rockfall characteristics in terms of maximum rebound height, translational velocity, and total kinetic energy. They also performed a comparative assessment by increasing the rock mass and slope height. Their analysis result showed that varying angles of slope geometry produced more problems than the rock mass in the rockfall scenario. Moreover, these researchers stated that nearly all of the rockfalls occurred because of the orientation and nature of discontinuities in the blocks. In the case of varying slope geometry, bounce height is more variable than the other parameters. However, as rock mass increases, bounce height increases with the same trajectory. Bounce heights exhibit complicated behavior as height increases. Consequently, the geometry of a slope is a more crucial parameter for rockfall compared with the mass of rockfall blocks.

15.11.3 Rockfall Analysis Using GIS-Based Models

Conventional information management related to rockfalls has typically been presented in report form, and photographs are generally organized into file folders and kept in filing cabinets. Data are arranged using indexing techniques to facilitate information search. At present, non-digitized methods cannot match our applications, and thus, introducing new techniques for information management is necessary; these techniques should consider information technology that comprises storage, acquisition, analysis, and distribution of information through a variety of electronic software and equipment products (Antoniou 2013). Information technology involves more than replacing file folders with electronic media; it completely changes the manner in which information is viewed and used. In geotechnical engineering, GIS application has focused on areas where data are defined spatially (Antoniou et al. 2008). GIS technologies and databases have been adapted for information storage associated with major geotechnical issues and their management (Fish and Lane 2002). At present, modern solutions for information technologies used in geotechnical engineering are not limited to stand-alone applications that have been developed in the past decades. However, integrating other sophisticated technologies, such as Web-based applications using the GIS environment and electronic data gathering, has produced modern techniques for the method, in which information is viewed and used in programming interfaces and applications to create maps and reports.

In the past decades, GIS has become a common technique utilized in managing and calculating natural hazards, including rockfalls (Pradhan 2010). GIS analysis has been widely proposed for generating rockfall hazard maps (Antoniou 2013). Rockfall models based on GIS are either raster-based modeling, for which input information are supplied via GIS analysis, or run within a GIS environment. Such rockfall modeling consists of three steps: identifying the rockfall source region in the zone of interest, determining the rockfall trajectory, and computing the length of run-out distance (Hegg and Kienholz 1995).

Lan et al. (2007, 2010) utilized a 3D extension for GIS to determine rockfall characteristics in terms of run-out distance, energy, and velocity. Inventory data were utilized to calibrate the mechanical parameters of the rockfall process. They proposed comprehensive methods for rockfall hazard assessment that considered the characteristics of rockfall source regions, the rockfall physical process, and the spatial attribution of rockfall energy and frequency. To evaluate the potential effect of rockfalls on railway operations, rockfall hazard distribution was investigated using rockfall frequency and energy-simulated distribution. They concluded that 3D rockfall modeling provides a fast framework for rockfall hazard assessment and for understanding the rockfall geomorphic process because it deals with 3D rockfall physical processes and the interaction of rockfall with slope topography. Moreover, it elucidates rockfall processes in terms of trajectory and dissipation as well as predicts their energy and frequency spatial distribution. To assess potential rockfall trajectories, Salvini et al. (2013) used the ArcHydro module of ArcMap and assumed that a rockfall would follow the direction of the steepest gradient. The morphological profile of rockfall trajectories was derived by interpolating 3D points obtained using a method developed in ArcInfo Workstation combined with the ArcMap Easy Profiler tool.

Jaboyedoff and Labiouse (2011) demonstrated that rockfall distribution regions could be specified by using a geometric rule known as the energy line or shadow angle technique based on a simple model of Coulomb friction performed in CONEFALL software. Run-out zones are evaluated from a DEM and a grid or cell file that represents probable rockfall source regions. Moreover, CONEFALL enables evaluation of maximum and mean rock energies and velocities in the rockfall distribution region. The identification of probable rockfall source areas is among the major difficulties in rockfall hazard assessment at a regional scale. Loye et al. (2009) studied probable rockfall source regions based on the distribution of the slope angle derived from a high-resolution DEM combined with other data obtained from topographic maps and geological GIS formats. The results showed that the predicted probable rockfall source areas match in situ observations conducted on test areas and derived from orthophotograph analysis.

Jaboyedoff et al. (2012a) used CONEFALL, which could simply implement a GIS environment, to assess run-out zones from potential source areas. Blahut et al. (2013) used both CONEFALL and RockFall Analyst (RA) codes in quantitative rockfall hazard and risk analysis to identify rockfall hazard regions. They concluded that RA could map rockfall hazard more realistically than CONEFALL in a variety of natural conditions, particularly within the studied region and provide realistic input data for risk assessment. The difference is attributed to the complex input information used in RA, which represents the local slope and energy loss coefficients of falling boulders. Moreover, CONEFALL calculations simplify the modeled rockfall by considering the sliding of rock blocks rather than their falling and bouncing.

15.12 Rockfall Trajectory Modeling Approaches

Rockfall trajectory codes can be categorized into 2D, 2.5D, and 3D rockfall trajectories models and adopt one of the simulation approaches. The analysis using the selected model can be performed probabilistically or deterministically.

15.12.1 2D Rockfall Trajectories Models

A 2D trajectory model simulates rockfall trajectory in a spatial domain determined by two axes. Such models can compute along the slope profile with user input based on distance axes (x, y) and an elevation axis (z) (Azzoni et al. 1995). Such profiles frequently follow the steepest descent line (Basson 2012). Another type of 2D model is rockfall trajectory, which is computed in a spatial framework determined through two distance axes (x, y), such as the contour lines of a map or the elevation values of a raster. This model typically computes the rockfall path using the run-out distance and velocity with sliding block and topographic–hydrologic methods. Gigli et al. (2014) used a 2D model to implement numerous rockfall simulations over the most crucial slope profiles specified through 3D modeling. Youssef et al. (2015) used 2D rockfall simulation software to elucidate the simulation of rockfall and define the main effect of falling rocks on neighboring regions. Antoniou and Lekkas (2010) used a 2D model under seismic and static loading circumstances in run-out distance analysis. Moreover, the selection of the 2D slope profile is critical to derive practical analysis outcomes using 2D rockfall models. Such models only produce a spatial representation of rockfall trajectory distribution because they require selecting critical 2D cross sections. In addition, such models are unable to

determine 3D rockfall process characteristics (Lan et al. 2007, 2010).

15.12.1.1 2.5D Rockfall Trajectory Models

A 2.5D model, also known as a quasi-3D model, is the second type of trajectory model and is basically a GIS-supported 2D model used to obtain pre-specified falling trajectories. This model separates the rockfall path direction in the (x, y) domain from the kinematics of falling rocks and rock trajectory along the vertical plane. To calculate the horizontal direction of falling in the (x, y) domain, this model divides the kinematics of rockfall calculation, bouncing heights, and positions. This condition indicates that this model performs two different 2D computations: defining the slope profile location in the (x, y) domain and simulating rockfall over the slope profile in 2D. An example of this model is one that calculates rockfall kinematics over a slope profile that follows the steepest gradient specified using digital surface information, such as the Rocky3 rockfall model (Dorren and Seijmonsbergen 2003).

15.12.2 3D Rockfall Trajectory Models

A 3D rockfall model is defined as a trajectory model that calculates rockfall path along a 3D plane (x, y, z) in each part of the calculation. Moreover, an interrelationship exists among rockfall trajectory direction in the (x, y) domain, the kinematics of a falling rock, its rebound height and position, and, if included, the influence of trees. The main advantages of 3D models include the converging and diverging effects of terrain and extraordinary or unexpected trajectories. However, 3D models require spatially evident parameter maps of the site, which are more time-consuming to prepare than the definition of parameter values for simulating rockfall trajectories based on slope profile (Volkwein et al. 2011). Examples of 3D models include rapid mass movements used by Leine et al. (2013) for rockfall dynamics, RA, a 3D rockfall process model integrated into GIS that enables effective handling of numerous geospatial information related to rockfall behavior used by Lan et al. (2007, 2010), Macciotta et al. (2011), Blahut et al. (2013), and Samodra et al. (2013, 2014) to assess rockfall characteristics in terms of run-out distance, energy, and velocity. Gigli et al. (2014) used RA to assess the effects of slope morphology on rock trajectory at a regional scale. Lopez-Saez et al. (2016) used a 3D rockfall trajectory model for four various dates to assess the effects of land use and land cover changes on rockfall propagation. The simulation permitted determination of return periods and rockfall kinetic energy, and consequently, the definition of associated hazards at the urban front for each time step.

15.13 Simulation Approaches

Rockfall simulation methods can be classified into three approaches: (i) lumped mass, (ii) rigid body (Hungr and Evans 1988), and (iii) the hybrid approach (Frattini et al. 2008). The following subsections discuss each approach.

15.13.1 Lumped Mass Approach

The lumped mass approach, which is the most widely used rockfall simulation method, considers falling rocks as point masses. Lumped mass models disregard the size and shape of a falling rock; moreover, the mass of the falling rock does not influence its trajectory but is used only to calculate energy. Lumped mass models simulate rockfall with different motion modes (flying, bouncing, sliding, rolling, and final deposition). They require two input parameters: the coefficients of normal and tangential restitutions (Rn and Rt) to compensate for the lack of physics applied in simplified models. The two coefficients of restitution parameters depend on several factors, such as the friction characteristics of falling rocks, incident angle, slope friction, and collision point in a falling rock with a non-spherical shape (Basson 2012).

15.13.2 Rigid Body Approach

Rigid body or rigorous models consider the volume and shape of a falling rock. However, considering the size and shape of individual rocks results in exaggerated computational demands that complicate the evaluation of a rockfall hazard at a regional scale (Guzzetti et al. 2002). The two input parameters in rockfall simulation based on a rigid body approach are dynamic friction (μ) and the normal restitution coefficient (Rn). Dynamic friction is the tangent line of the frictional angle that can be derived from empirical data. Chai et al. (2013) demonstrated that the empirical parameter Rt could be derived via rigid body impact mechanics using only the material parameters Rn and μ. They also introduced the influences of rock size and shape, as well as their interactions with the slope, to compute rockfall trajectory and derive Rt.

15.13.3 Hybrid Approach

The hybrid approach combines with the other two approaches such as using rigid body approach in order to simulate rolling, impact and bounce and lumped mass approach in order to simulate free fall (Frattini et al. 2008).

15.14 Parameters for Rockfall Analysis

The parameters required to simulate rockfalls can be divided into two groups: geometric parameters (seed point identification, topography, outcropping material limit, location of points of interest, or elements at risk) and mechanical parameters (coefficient of restitution (COR), roughness, and friction angle) (Gigli et al. 2014). The most significant parameter is COR. Geometric properties are derived from field elevation observations, whereas mechanical–physical characteristics can be obtained from in situ and laboratory tests or from the implementation of back analysis (Firpo et al. 2011). The trajectories of rockfall, bouncing height, and impact energy rely on slope surface roughness, slope geometry, and rockfall block characteristics (Arbanas et al. 2012). The mass of a rock considerably influences impact energy, such as the kinetic energy of a block, which consists of a smaller rotational component and a translational component. Therefore, rigorously and accurately characterizing a potentially unstable rocks mass or size in a particular field is important (Spadari et al. 2013). Moreover, rock slope geometry significantly affects the post-impact behavior of falling rocks. Slope geometry is vital in any rockfall analysis. Its effect adds a dimension to the final impact distance variation (Vijayakumar et al. 2011). The identification of probable rockfall source regions is a difficult task in rockfall prediction. Source zones are frequently obtained from apparent evidence, such as the deposition of a talus slope below a cliff face, field measurements, and historical register information. Rocky outcrops, and consequently, unstable rockfall source areas are mostly found on steep slopes (Jaboyedoff et al. 2012a).

15.14.1 COR

COR describes the kinematic behavior of a falling rock as it hits the slope surface. Every time a rock hits a slope surface, its movement characteristics are changed. Hoek (2007) described COR as the mathematical expression of the retarding capacity of a surface material when dealing with falling rocks. Each slope has unique properties that vary among regions along the slope. Each falling rock also has unique properties. Therefore, characterizing COR is difficult because each case has a unique set of properties. To simplify this process, COR is generalized to fit the behavior of similar falling rocks downslope with known parameters. Rn is a classic parameter. It denotes material characteristics, which are determined by contacting slope rigidity. Meanwhile, Rt is an experimental parameter that is measured using slope material and vegetation. The range of the proposed Rt value is relatively larger than the range of the proposed Rn value. For example, the proposed Rn values of firm soil and talus slope range from 0.1 to 0.2, whereas their proposed Rt values range from 0.5 to 1.0 (Chai et al. 2013). In another paper, Vijayakumar et al. (2012) used a simple mechanical model to demonstrate that the computed Rn had a value greater than 1.0; this trend, which is evident in certain rockfall field data, is caused by the eccentricity of rock shape and its rotational energy. Their group also demonstrated that the computed coefficient can become negative in some cases. Although such cases seem to break the law of energy conservation, the appropriate description is found in the definition of COR itself. In most situations, the rock body is a point mass; thus, Rn must be based on the incoming and outgoing velocities of the center of mass. Otherwise, the rotating energy is unaccounted for in the point mass model.

The values of COR may vary considerably, depending on the site conditions. Therefore, the two components of COR (normal and tangential) have to be determined separately for each field. The in situ test or back analysis of falling rocks can be used to derive COR. The most critical input parameters for simulating rockfall phenomena are CORs, which control the bouncing of rocks (Asteriou et al. 2012). Chau et al. (2002) presented the results of an experimental study on COR for spherical blocks that affected a rock slope. A plaster modeling material was used to cast both the slopes and the blocks. A positive correlation was noted between slope angle and Rn. However, no apparent relation was detected between slope angle and Rt. When the resultant velocity ratio and kinetic energy ratio before and after impact were utilized to define COR, COR evidently increased with slope angle.

The physical or mechanical parameters (COR and friction angle) are particularly significant inputs for rockfall simulation; these factors control block bouncing, velocity magnitude, and rockfall trajectory analysis (Asteriou et al. 2012; Lato et al. 2012). In addition, the loss of rock boulder energy upon impact is controlled by COR (Keskin 2013; Samodra et al. 2014; Sabatakakis et al. 2015). In principle, hard materials exhibit higher CORs than soft materials. Moreover, Rt increases with Rn. Slight changes in COR values cause entirely different trajectories.

COR is one of the most significant and most difficult parameters for assessment in rockfall analysis (Papathanassiou et al. 2013). However, these values may vary dramatically, depending on the circumstances of each site (Topal et al. 2007). These values also differ for diverse materials and various types of vegetation covering the slope; in addition, the values are dissimilar within the same environment (Macciotta et al. 2014). To avoid obtaining irrelevant values, coefficient distribution can be truncated between the

important minimum and maximum values (Frattini et al. 2013). Attempts to model rock-ground effects using a single COR do not sufficiently capture rockfall variability (Glover et al. 2015). Moreover, the slope friction angle cannot be derived via field testing (Ku 2012).

The most commonly used definitions of COR components (normal and tangential) are

$$\mathrm{Rt} = V_{\mathrm{tr}}/V_{\mathrm{ti}}; \quad \mathrm{Rn} = V_{\mathrm{nr}}/V_{\mathrm{ni}} \tag{15.2}$$

where V_{nr} and V_{ni} are the quantities of the rebounding and incoming velocities of the normal component, respectively; and V_{tr} and V_{ti} are the quantities of the rebounding and incoming velocities of the tangential component, respectively (Fig. 15.4).

Chiessi et al. (2010) performed rockfall hazard assessment using two individual approaches. The analyzed rockfall trajectories is strongly affected by the input parameters, particularly the COR values. Asteriou et al. (2012) performed in situ and laboratory tests to determine the parameters that affected rockfall trajectories. CORs are the most critical parameters in rockfall modeling. Wyllie (2014) documented rockfalls in five locations, including the effects on rock, talus, colluvium, asphalt, and concrete. The values of Rn and Rt were calculated for these locations. The field results showed that Rn was related to the impact angle. The Rn values are essentially independent of the slope material. The Rt values ranged from 0.3 to 0.8. This coefficient is related to the friction coefficient at the impact point. Its value is independent of the velocity and normal force. The calculated field values for CORs are consistent with the principles of impact mechanics.

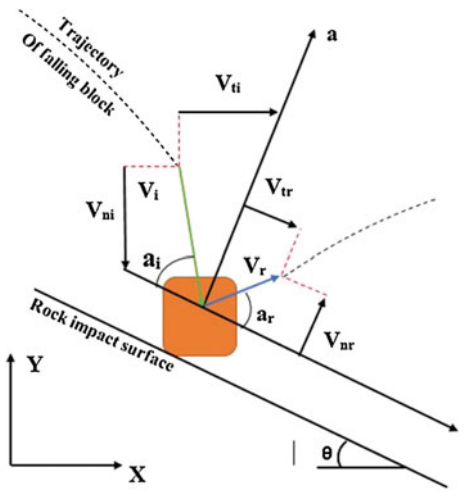

Fig. 15.4 Components of translational velocities before and after impact (Asteriou et al. 2012)

15.15 Possible Measures for Mitigation of Rockfall Hazard

15.15.1 Potential Rockfall Problem Identification

The identification of all probable rockfall hazards using common techniques for rockfall hazard assessment is neither practical nor possible. For example, when studying the blocks on the highest slope portion, rockfall hazard is apparent. Nevertheless, the most hazardous types of rockfall occur when a rock is suddenly detached from a cliff face through comparatively small deformations in neighboring rocks. This event may happen when a force affects discontinuity across planes, thereby separating a rock from its surrounding. A change in discontinuity is attributed to water pressure or the reduced shear strength of planes because of long-term damage after weathering. This phenomenon can sometimes trigger rockfalls of considerable sizes or, in excessive cases, large-scale slope failures. Rock faces should be accurately examined for probable rockfall problems. However, not all rockfall hazards will be revealed through this examination.

15.15.2 Decrease in Energy Level Related to Excavation

Conventional excavation techniques for rocky slopes include blasting. Even with controlled and planned explosions, high-intensity forces affect rock masses for a short period. Wedges and blocks may be triggered by such strong forces. Therefore, to reduce rockfall hazard caused after excavation by explosion, another method should be used; for example, ripping requires concentrated vibrations or short-period forces on rock masses. Manual and mechanical excavation techniques can also be utilized. When an enormous amount of rocks need to be destroyed, chemical expansion may be used.

15.15.3 Physical Restraint of Rockfalls

Rockfalls vary spatially and temporarily; thus, detecting all rockfall hazards is impossible. Techniques for reducing the effects of these rockfalls hazard must be considered. These techniques are elucidated in Fig. 15.5.

A berm is a relatively efficient method for catching rockfalls; this structure is commonly utilized on a permanent slope. Nevertheless, berms may be excavated from the top down. During construction, the use of berms is limited in

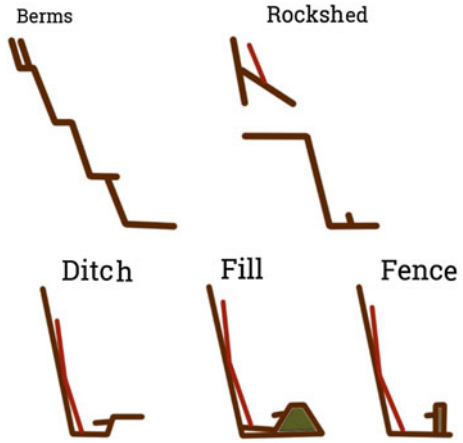

Fig. 15.5 Possible techniques to reduce the damage due to rockfall, after Spang and Rautenstrauch (1988)

minimizing rockfall hazards. Avalanche shelters or rocksheds are frequently utilized over a steep slope above a narrow roadway or railway. A steep slope roof coverage with a comparatively narrow extent is required for efficient shelter. For a wide multi-lane expressway, designing a rockshed structure with an adequate capability to resist large rockfalls may be impossible. In general, a fill of soil or gravel is recommended at the top of a rockshed to function as a rockfall deflector and retarder. Rock traps can effectively catch rockfalls by providing an adequate room at the slope toe to accommodate such trap. In the case of a relatively narrow highway at a steep slope toe, adequate room for rock trap accommodation is difficult to find. Frequently utilized barriers or catch fences are estimated to have an energy absorption capacity of 100 kN/m^2. This value is equal to a 250 kg rock mass falling with a velocity of approximately 20 m/s. However, a robust barrier fence can have an energy absorption capacity of up to 2500 kN/m^2, which can stop a 6200 kg rock moving at a velocity of approximately 20 m/s. The use of a mesh draped over a rock face is another restraint technique that deserves further consideration. Meshes extend along a rock face and are attached at several positions over the slope surface. A mesh is not used to stop rockfalls but is intended to trap the falling blocks between the rock face and the mesh, thereby reducing rock velocity that causes rocks to bounce out onto the highway. The construction of a catch ditch at a slope toe is probably the most efficient permanent rockfall protection technique for most expressways. To increase the efficiency of ditches, a ditch base is normally covered with a gravel layer for the energy absorption of falling boulders; a robust barrier fence is placed between the highway and the ditch. The location of a barrier fence can be assessed based on rockfall analysis, such as rockfall trajectories and their characteristics.

15.16 DEM

A DEM is a 3D representation of a topographical terrain. Current geomorphometry focuses on the parameters obtained for a terrain surface (slope, slope aspect, and curvature) and the spatial features or land surface objects (cirque, watershed boundary, and drainage network) from DEM. This characterization depends on the general and specific geomorphometric analysis modes. Specific modes describe discrete surface objects, such as landforms, whereas general modes describe a continuous terrain surface. The most typical data format is the DEM square grid, where the gridding sets of points in Cartesian spaces are assigned with elevation values that characterize the terrain surface (Wilson 2012).

A DEM provides basic information about topographic relief. The resolution of this model significantly affects modeling outcomes, thereby indicating that its selection is a critical step in the numerical modeling of rockfalls (Salvini et al. 2013; Bühler et al. 2014). This finding is attributed to the reliable prediction of such events, which is highly relevant to the 3D characteristic of real slope geometry (Ku 2012). In particular, LiDAR techniques may be applied in rockfall hazard assessment because of their capacity to produce precise and accurate ground surface DEMs (Rayburg et al. 2009; Barbarella et al. 2013). Bühler et al. (2014) used high-resolution LiDAR (50 cm) to sample the land morphology of an extremely active rockfall region. Their group resampled the obtained DEM into various resolutions. Rockfall simulation was conducted while the terrain effect parameters of the model were kept fixed. In addition, the release orientation was varied to mimic the naturally stochastic initial circumstances of boulder fall detachment, whereas potential energy was kept fixed. The various results of rockfall simulation were compared to assess the effect of DEM resolution on completely 3D rockfall simulation. DEM resolution significantly affects the results of rockfall simulation, thereby demonstrating that DEM selection is a crucial part of numerical rockfall simulation.

15.16.1 DEM Data Acquisition

DEM production integrates three correlated functions: (i) terrain surface sampling, such as the collection of altitudes; (ii) surface model generation from the sampled altitudes; and (iii) error correction in the generated DEM (Hengl et al. 2010). Data sources and processing techniques for creating DEMs have developed rapidly from a topographic map and land survey transformation to passive remote sensing techniques and more recently to active remote sensing techniques using radar and LiDAR (Wilson 2012). DEM can be derived from different sources with various spatial resolutions ranging from a few centimeters to 90 m.

DEM spatial resolution that symbolizes surface topography can considerably influence the results of rockfall simulation. In particular, the terrain roughness of a boulder field or a scree slope is included when the spatial resolution of DEM (centimeters to meters) is fine (Bühler et al. 2014). Nelson et al. (2009) classified DEM data into three general classes based on collection methods: (i) land survey methods involving theodolite, electronic distance measurement (EDM), total stations, and global navigation satellite system (GNSS) instruments; (ii) existing topographic maps, which are in hardcopy form, including the elements of contour lines, lakes, rivers, and spot heights; and (iii) remote sensing techniques, including airborne and satellite photogrammetric techniques, airborne and terrestrial laser scanning, and airborne and satellite radar.

15.16.2 Pre-Processing of Data and DEM Construction

The preparation of elevation data for geomorphometric analyses is a complex process because elevation itself is generally not the attribute of concern. The actual geomorphological accuracy may be evaluated using terrain parameters and feature measurement, including landforms or in-site drainage lines and the comparison of their locations, distributions, and shapes with data derived from geomorphometric analyses (Wilson et al. 2008). Reuter et al. (2009) proposed that the actual application of DEMs in geomorphometric analyses could be evaluated by answering the following questions. (i) What is the terrain roughness representation accuracy? (ii) What is the accuracy of representation of the ground surface shape (i.e., convex and concave shapes, water divergence or convergence, deposition, and erosion)? (iii) What is the accuracy of detection of streamlines and world ridgelines? (iv) How regularly is elevation measured over the entire concern area? The responses to these questions and other comparable queries are interconnected. Errors will be mostly present in the preferred or accessible DEM despite the responses to these significant queries. Error magnitude and frequency depend on the methods and techniques utilized for data gathering, the implemented algorithms in pre-processing, and ground surface characteristics.

Elevation data resolution (horizontal and vertical) was utilized to describe ground topography. These data definitely have a major effect on the information level and the accurate description of terrain objects, as well as on the values of the terrain surface parameters, which are calculated from a DEM (Bühler et al. 2014). Grid spacing also influences the accuracy and values of landform objects and the parameters of land surface (Raaflaub and Collins 2006). The rapid development of mass-produced sources and remote sensing DEMs over the last two decades requires new techniques for DEM pre-processing. Webster and Dias (2006) and Reuter et al. (2009) described varied approaches and possibilities for orthorectifying DEMs, reducing local noise and outliers, filtrating water surface, filtrating clear noise, filtrating forests in DEM, filling sinks and voids, mosaic neighboring DEM, and filtrating LiDAR DEM.

Before producing the triangulated mesh required to generate a DEM of the cliff surface from the obtained point cloud, a pre-processing step has to be performed, including two major functions: (1) eliminating vegetation cover and (2) differentiating rock outcrops from the construct surroundings and the detritus at the slope toe within the point clouds. The decimation and segmentation stages are implemented using manual and automated methods; point cloud filtering based on the various intensity of the pulse return is reflected from the scanned features (Fanti et al. 2013). This tedious pre-processing of point clouds is justified by the eventual objective, i.e., the generation of a dependable DEM that is appropriate for rock mass discontinuity characterization. In general, non-geological and vegetation points, as well as registration error, can contribute to noise in point clouds and influence the procedure of automatic meshing (Buckley et al. 2008). After point extraction on a rock mass out-crop, the resultant points can be resampled to obtain a uniform and regular spatial distribution. To create continuous surfaces from discrete information, the sampled point clouds can be eventually triangulated by considering the fill holes to produce homogeneous surfaces.

15.16.3 Computation of Terrain Parameters

In the regular workflow of digital modeling, the focus will be on obtaining spatial features (land surface objects) and the values of terrain parameters after an appropriate DEM is produced. The parameters of a terrain surface are directly obtained without further input from the DEM. To characterize these parameters, various terms are utilized in the literature. Olaya (2009) defined these parameters as "basic" parameters of terrain surfaces; these parameters could be computed from a DEM without additional comprehension of the explained region. Florinsky (1998) differentiated local elementary attributes that were computed as a function of their neighboring and regional elementary attributes, which required a wide regional ground surface area analysis from a computing approach. Wilson and Burrough (1999) demonstrated the differences between the regional and local surface characteristics of the presence of local interactions between "action-at-a-distance" forces and surrounding points. The parameters of the local land surface included aspect, slope, and curvatures; the parameters of regional ground surface included the extent of flow trajectory, downslope contribution area,

dispersion area, and the proximity to the closest ridgeline. Most local parameters are calculated through a (3 × 3) window approach moving over a grid and computing the parameters of the land surface for the concerned cell, i.e., the centric cell of the (3 × 3) window (Fig. 15.6). Specific principles are available on how to deal with this approach; the edges create a new raster for each parameter, which has the same size as the DEM. Various formulas have been presented for calculating aspect and slope as the first extraction and curvatures as the second extraction (Florinsky 1998; Shary et al. 2002).

The computation and interpretation of the aspect and slope grids are reasonably uncomplicated. The vertical curvature or profile and the horizontal curvature or tangential are frequently utilized to differentiate locally concave and convex shapes. In geosciences, the curvature sign is written by convention as negative and positive for concave and convex shapes, respectively (Olaya 2009). That is, concave and convex tangential curvatures represent the convergence and divergence of flow paths, respectively. The concave profile curvature represents slope flattening, and thus, a decrease in potential energies. By contrast, the convex profile curvature represents flow acceleration, and consequently, a local increment in potential energies. Finally, the scale issues with the framework of the land surface parameters should be addressed. Local land shapes frequently exhibit a constant difference in altitude values from point to point over land surface; these shapes significantly influence regional and local ground surface characteristics. However, this role is affected by data and processing factors. Florinsky (1998) reported that local attributes, such as aspect, slope incline, and curvature, were mathematical variables instead of actual values. This assertion can be expanded to all local ground surface characteristics because of two reasons. First, the shape of the local ground surface can depends on various mathematical descriptions; thus, computed local attributes depend on the selection of the algorithm. Second, the terrain shape represented by DEM is a scale function, which is combined with terrain complexity, spatial scale, and resolution or scale of data from which the land surface is observed.

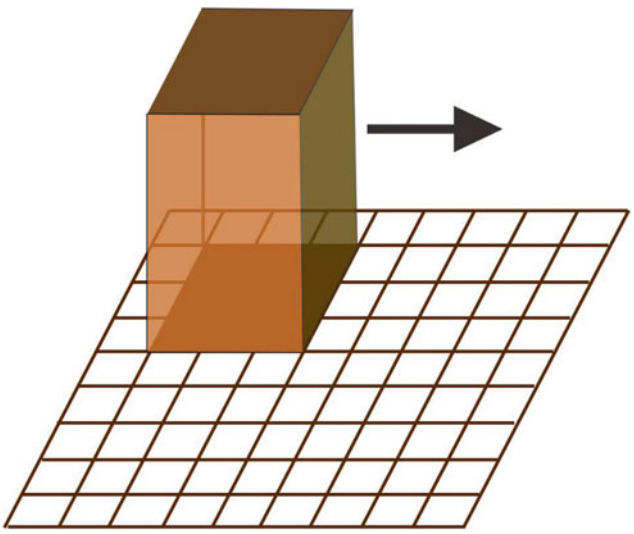

Fig. 15.6 Terrain parameters are typically computed by moving a 3 × 3 grid across a DEM (Olaya 2009)

15.16.4 Error Calculation in DEM

Errors in DEM are variable, depending on the sensor selection or particular application (distribution technique); thus, a DEM will be deduced from another to present elevation difference for evaluating deposition, erosion, and change (Burns et al. 2010). The other group of difficulties is related to altitude error propagation in terrain parameters, and considerable effort is frequently required for error identification. Nevertheless, errors associated with the data source are mostly difficult to remove; any individual concerned with utilizing terrain surface parameters derived from DEM should be aware of these errors and how these errors may influence workflow and interpretation, and consequently, the results. Several methods have been presented to evaluate the accuracy of DEM altitude values (Temme et al. 2009).

Several researchers have compared a series of altitudes obtained from a DEM and the actual altitude values derived from the most precise sources of topographic information; the root-mean-square error (RMSE) of altitude, which represents the variation between true and derived values, has also been calculated (Wise 2000). The only issue with this method is that it disregards the spatial distribution pattern and the existence of systematic bias of errors, which are crucial to these terrain surface parameters (Hutchinson and Gallant 2000). The aforementioned parameters are significantly affected by the shape of the terrain surface. Carara et al. (1997) proposed multi-criteria with broader significance to assess the quality of a DEM created from contour lines. The values of the DEM and contour lines should be similar and close to the contours. The values of the DEM should be within the range specified throughout an interval of contours. The values of the DEM should nearly linearly differ with the values of the contour line interval. Artifacts have to be restricted to within a small portion of the data set, and DEM patterns should reflect the actual shape in flat areas. Hutchinson and Gallant (2000) measured the quality of a DEM, which was created from surface contour lines; point elevation and streamlines data suggested a wide and more varied list of simple metrics that included some of the same schemes. Abellán et al. (2009, 2010) applied a nearest neighbor (NN) averaging technique to minimize the error in

RAW data obtained using the LiDAR technique. The NN method is composed of three steps: (1) interpolation of data to a square grid or cell, (2) search for the n neighboring points, and (3) the NN average value calculation for each point, except for the edges. The selection of the DEM interpolation technique can strongly influence DEM surface properties (Wise 2011; Gallay et al. 2013). Bater and Coops (2009) examined seven interpolation procedures using airborne laser scanning (ALS) data. These data were categorized from random subsets into a verification data set and a prediction dataset. A series of DEMs was generated through the natural neighbor, linear, regularized spline, quintic, spline with tension, inverse distance weighted, and finite difference approach interpolation algorithms. These researchers concluded that the natural neighbor interpolation algorithm provided the best outcomes at minimal effort among all the algorithms.

15.16.5 Remote Sensing Techniques for Capturing DEM

The topography of complex landscapes is challenging to obtain in remote regions; moreover, ground-based survey techniques can be difficult, time-consuming, and less/insignificant landscape features. DEM can be generated from various data sources, but this diversity can result in different precision and accuracy degrees. Remote sensing and GIS have revolutionized hazard studies because of their efficient data collection, analysis, and validation processes (Pradhan et al. 2011). During the last two decades, the rapid development of data sources for produced DEMs, such as photogrammetry, shuttle radar topographic mission (SRTM), radar interferometry (InSAR), and LiDAR surveying, has considerably improved DEM resolution because of the highly accurate and precise data that they can provide.

15.16.5.1 Photogrammetric-Based DEM Generation

Photogrammetry provides 3D point coordinates with expected accuracy from stereo- or multi-photographs, such as from photographs taken for the same scene from various viewpoints. The accuracy of the coordinates relies on the number of elements that should be considered in designing the steps for any photogrammetric surveying: the calibration of the camera, the orientation of photographs, and the restitution of objects. Object-based photograph construct and matching from the movement, extraction, and matching of tie points can be automatically performed; thus, the orientation of a photograph can be derived without any manual measures. The parameters of orientation can also be specified immediately through the fixation of a GNSS device, incorporated with an inertial measurement unit (IMU) and a camera. This combination allows processing without requiring ground control points (GCPs). The restitution of an object can be performed automatically or manually by a technician. Photogrammetry has a long history among remote sensing technologies for DEM production. Photogrammetry techniques have confirmed their efficiency for an extensive range of mapping applications, including the production of DEMs, cartographic maps, and orthophotographs. Photogrammetry is commonly utilized as a multipurpose spatial data-capturing technique given the rapid development in the utilization and maturation of GIS. Figure 15.7 illustrates a 1 arc-second (30 m) photogrammetric DEM. DEM generation based on photogrammetry principles has two operating phases: the initial measuring phase and the second phase for DEM derivation. The primary data sources are from aerial photographs (film-based or digital). Digital image-processing techniques are applied by interacting (user-based) measured techniques or an automatic technique. The DEM points identified by the interpolation process from the aerial photographs (stereo pairs) are based on object matching (Chang et al. 2004).

Photogrammetry based on repeated aerial photography is considered an adequate remote sensing technique for long-term monitoring of small deformation rates along large regions (Strozzi et al. 2010). Terrestrial photogrammetry is another type of photogrammetry; this method is beneficial for performing elaborate surveys of geometric–structural environments, even in unreachable areas. Firpo et al. (2011) used various terrestrial photogrammetric techniques for rockfall simulation. Their result demonstrated that the quantity and accuracy of geometric and geological information acquired from a photogrammetric survey permitted the numerical assessment of the correlation between rock factors as a function of their load conditions and mechanical or physical properties. In addition, potential shadow can be removed by varying the focal length and shooting position. Nevertheless, this survey technique has drawbacks, such as in extremely high slopes, where a full photogrammetric survey of the highest regions of a rocky wall is impossible to perform.

15.16.5.2 SRTM DEM Generation

The 3 arc-second SRTM DEM, which has been developed based on satellite data gathered during a nine-day window in 2000, includes a considerable portion of the world (58°S to 60°N). This dataset is recognized as one of the most proportionate, perfect, and common environment datasets worldwide (Zandbergen 2008; Nelson et al. 2009). The spacing of 3 arc-second grids (~90 m) is preferable compared with the worldwide GTOPO30 DEM spacing of 1 km. An accuracy evaluation using kinematic GNSS data demonstrated elevation accuracy, where 90% of the errors were less than 5 m (Rodriguez et al. 2006). Recent studies

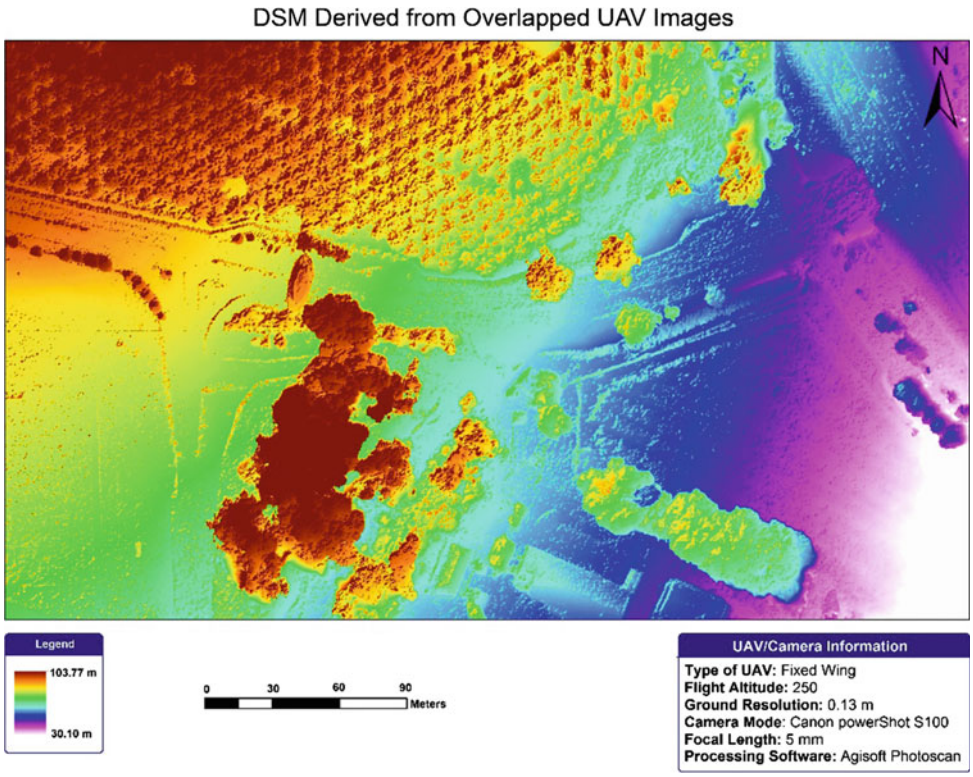

Fig. 15.7 A 1 arc-second photogrammetric DEM (Chang et al. 2004)

have demonstrated a positive correlation between elevation error and canopy height (Hofton et al. 2006; Berry et al. 2007). The relatively new technique of Advanced Spaceborne Thermal Emission and Reflectance Radiometer Global DEM (ASTER GDEM) was released in 2009. The ASTER GDEM technique provides greater spatial covering (83°N to 83°S vs. 60°N to 58°S) and higher resolution (1 arc-second vs. 3 arc-seconds) as well as comparison of the horizontal and vertical accuracies for SRTM (Nelson et al. 2009; Slater et al. 2009). Furthermore, the issues of missing data due to cloud are considerably easier to fill. Nevertheless, a 30-m resolution is still inadequate for supporting vegetation, soil mapping, and related phenomena in most terrain.

15.16.5.3 InSAR DEM Generation

Synthetic aperture radar (SAR) is defined as a side-looking active radar range technique. SAR utilizes the microwave part of the electromagnetic spectrum, including frequencies ranging from 0.3 to 300 GHz or from 1 mm to 1 m in the wavelength range. InSAR requires two SAR photographs for the same location. Those photographs can be obtained separately at the time of revisiting the same location with a single antenna, such as in a typical spaceborne radar system or while simultaneously utilizing two antennas hanging on a platform, such as several satellite and typical airborne systems. Both photographs are then registered accurately with each other to calculate the phase variance between the pixels in the two photographs. This interferogram or phase variance can be utilized to obtain the DEM of the captured region. Figure 15.8 illustrates an InSAR DEM obtained from the images of the European remote sensing satellite (ERS)-2 and ERS-1 captured during the "tandem" mission (Chang et al. 2004). ERS SAR works with an incidence angle $\theta = 23°$ from the vertical direction at the center of the swath, which is 100 km wide, and at the wavelength $\lambda = 5.65$ cm. SAR revisits a particular location every 35 days.

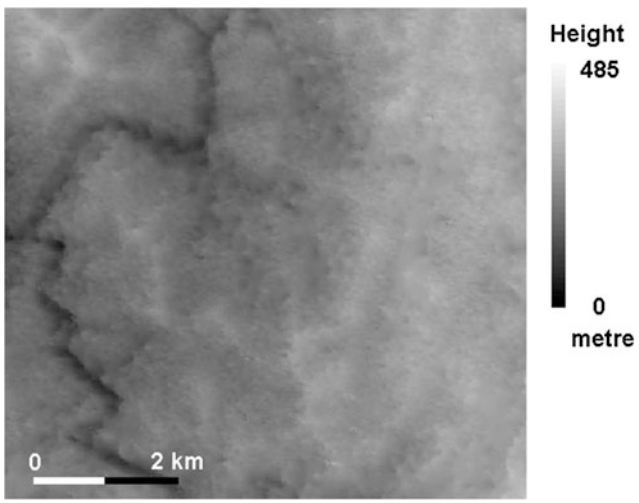

Fig. 15.8 InSAR tandem DEM

15.16.5.4 Unmanned Aerial System (UAS)

A UAS is known by various terms and names, such as aerial robot, drone, or unmanned aerial vehicle (UAV); the most popular acronym is UAV. A UAS is composed of three basic components, which are frequently defined as the unmanned aerial vehicle, the communication and data link, and the ground control station. Furthermore, other components of UAS are considered crucial, such as navigation sensors, autopilots, mechanical servos, imaging sensors, and a wireless system. DEMs and orthophotographs are two major UAS products. At present, a UAV can be utilized to accelerate the external direction phase and minimize operational cost. The main usefulness of UAV-based remote sensing applications for dangerous environments such as rockfalls, landslides, or mudslides is their capability to obtain data in hazardous regions of concern. Direct measurements in such areas are frequently impossible. The flying motion of a UAV is autonomously based on a programmed plan of flight that utilizes compound dynamic automated systems and GNSS/INS to guide external directions. The processing of a DEM creation basically relies on several elements, such as flight height, overlapping, and camera resolution. The differences in these factors influence the final accuracy of the obtained results. The standard algorithms for DEM creation suffer from normal errors caused by GNSS/INS instruments, particularly in location measurement related to each obtained photograph. The difference between real locations and these measurements is approximately a few meters. The complete flowchart of DEM generation algorithms is depicted in Fig. 15.9 (Ruiz et al. 2013).

The regular products of UAVs are dense DEMs of approximately 50 points per square meter, 2 cm seamless orthophotographs, and 3D vector maps with a 2 cm point precision in XY and 4 cm in altitude (Haarbrink and Eisenbeiss 2008). Hand-launched and simple UAVs that operate autonomously by utilizing its GPS-driven autopilot and, typically, an IMU sensor, are the most affordable systems. Nevertheless, most of these systems are significantly influenced by cold and wind, and thus, they are rarely utilized or difficult to utilize in mountainous topography (Niethammer et al. 2012). The most stable systems, generally those with a gasoline engine, have greater payloads and allow a more professional camera onboard or even conduct surveys using LiDAR instruments. Fritz et al. (2013) compared LiDAR point clouds and UAS-based point clouds by utilizing a frame camera for tree trunk reconstruction. The resulting points with reconstruction were less dense and less accurate than with LiDAR. In addition to the frame camera, the LiDAR technique plays a major role in point cloud creation. However, the use of LiDAR techniques in UAS platforms for DEM generation remains infrequent. Niethammer et al. (2010) used a UAV for high-resolution acquisitions of landslides. Digital surface models (DSMs) have been generated from the airborne photographs of a landslide using a modern features-based surface reconstruction technique that does not require any GCP information.

Giordan et al. (2014) used a micro-UAV in an emergency scenario related to rockfall phenomenon. The 3D photographs derived were utilized to create the first-order DSM, which provides quantitative information about the orientation and the dimension of the main discontinuity identified in the rock mass. The LiDAR technique was used to acquire a high-resolution DEM of the study area to improve and validate the results derived from micro-drone surveying.

15.17 Detection and Characterization of Rock Mass Movement

ALS and terrestrial laser scanning (TLS) technologies are responsible for the outstanding development in the characterization of rock slopes, primarily because rock instability are mainly dominated by a structure that is at least locally

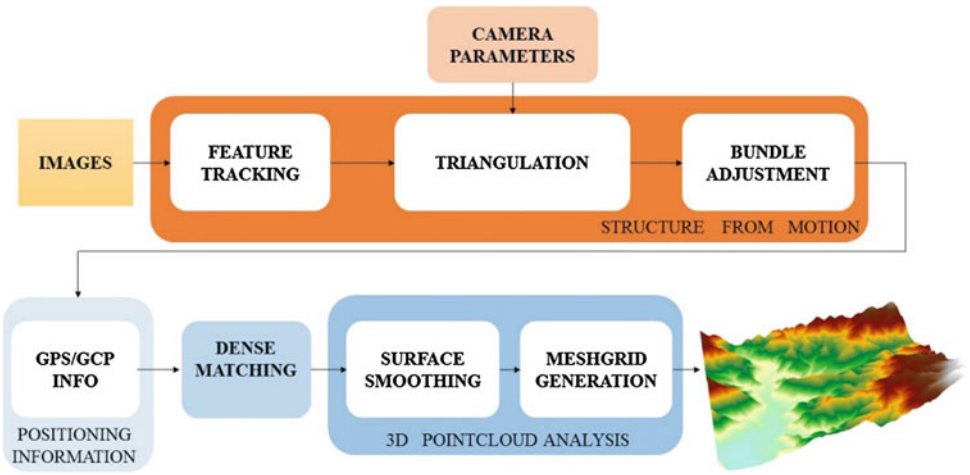

Fig. 15.9 DEM generation algorithms (Ruiz et al. 2013)

plane surfaces. The applications of TLS in rock mass characterization are countless (Oppikofer et al. 2009; Sturzenegger and Stead 2009; Lato et al. 2009a, b; Armesto et al. 2009). By contrast, the applications of ALS in generating DEMs are still uncommon.

15.17.1 Using ALS

Large-scale feature analyses are required to derive DEMs by utilizing ALS based on the COLTOP principle (Jaboyedoff et al. 2009b), which permits assigning a distinctive color to each topographical direction. This technique also enables rapid feature characterization of inaccessible areas (Brideau et al. 2009) and the reinterpretation of previous rockfalls (Froese et al. 2009). Oppikofer (2009) investigated a fiord valley at the regional scale to characterize the instability of former and present rock slopes, i.e., their mechanisms and volume.

15.17.2 Using TLS

The TLS characterization of a rock slope is one of the first applications that utilize TLS for slope mass movement, mostly to acquire accurate discontinuous orientations and slope profile (Bornaz et al. 2002; Slob et al. 2002). The various methods for characterizing discontinuity sets can be divided into three parts. The first part involves the use of the appropriate plane (Abellan et al. 2006; Sturzenegger and Stead 2009). The second part utilizes the triangular irregular network (TIN) surface as an indicator of plane orientation (Feng et al. 2001; Slob et al. 2002). Kemeny and Post (2003) provided a description of this methodology for rock mass characterization using Split-FX software. Lato et al. (2009a, b) demonstrated the optimum point number for point clouds to obtain a realistic result based on the precision level of the instrument. Furthermore, a high-density TIN is influenced by data noises. Finally, the other methods enable the automatic delineation of a set of neighborhood points, which are characterized by the same normal vector. Consequently, the computation of the orientation of plane discontinuities is acquired.

The COLTOP method allows visualization of each discontinuity orientation set by using a distinctive color that makes the method similar to in situ data capturing (Jaboyedoff et al. 2009b). The obtained data allow the analysis of rock instability mechanisms (Oppikofer et al. 2009; Janeras et al. 2004). Lato et al. (2009a, b) and Sturzenegger and Stead (2009) noted two types of bias in the definition of discontinuity orientation: (a) a scale bias is observed when spatial resolution (point spacing) is larger than the discontinuity sets and (b) an orientation bias is observed when the spatial resolution is influenced by the incidence angle of a given data set. Roughness determination is another aspect of the application that is integrated into rock slope characteristics. Haneberg (2007) and Tatone and Grassel-li (2009) attempted to improve the quantification of popular techniques for rock mass rating systems. However, certain limitations are associated with the achievement of this goal, such as the inherent instrumental accuracy and the resolution of various scanner locations on the eventual outcomes (Sturzenegger et al. 2007).

15.18 Rockfall Monitoring

The monitoring of surface displacements in a rocky slope is easier than in soil slopes because the displacement can be regarded as rigid body transformation (Monserrat and Crosetto 2008; Oppikofer et al. 2009; Abellan et al. 2009). Thus, the movements are considered a combination of translation and rotation in various slope portions. Detailed movement analyses that utilize the rigid body transformation method combined with comprehensive structural analyses enable the determination of potential rockfall mechanisms (Oppikofer et al. 2009). The possibility linkage of temporal and spatial rockfall predictions represents a considerable challenge in the monitoring of rockfalls. Recently, two various preliminary indicators were investigated: (a) the increase in rockfall activities prior to final collapses (Rosser et al. 2007) for a hard rock cliff and (b) preliminary displacement detection was investigated for a large rockfall (Oppikofer et al. 2008) and fragmental rockfalls as Abellan et al. (2009, 2010) illustrated that few centimeters displacement prior rockfall with few to hundred cubic meters. Although the magnitude of preliminary displacement can be same as that of instrument errors in some cases, several researchers have noted that these errors can be considerably reduced by considering the information from the adjacent points, such as in cases of filtering noise reduction or averaging (Monserrat and Crosetto 2008; Abellan et al. 2009). Abellan et al. (2009) demonstrated the possibility of millimetric terrain displacements detection in outdoor experiments, even with a single point, which had the highest standard deviation.

15.19 Rockfall Analysis

Traditional surveying techniques present significant restrictions in acquiring spatial datasets required for rockfall assessment. The use of modern technologies, such as LiDAR, has rapidly improved in the field of geohazard evaluation. ALS and TLS surveys are currently considered essential tools for accurate and dense information collection to assist detailed topographical analysis. From a deterministic perspective, rockfall trajectory depends on (1) the

location point at which the rock detaches, (2) the rock that is detached, (3) the slope properties, and (4) how the rock behaves over slope surface (Salvini et al. 2013). The first elements correlate with the source position (i.e., plane coordinates and altitude) (Li and Lan 2015).

DEM resolution significantly influences detection of rockfall sources: a rough DEM tends to smooth the values of the slope angle (Michoud et al. 2012). Loye et al. (2009) reported that the higher the DEM resolution, the smaller the probable source regions. Moreover, the rougher the DEM, the lower the evident slope angle. For example, for a 10 m DEM, the apparent vertical cliff slope angle is 55°, whereas it is 83° for a 2 m DEM. The accessibility of a high-resolution DEM at a regional scale facilitates detailed terrain analysis. Thus, a DEM-based geomorphometric approach accurately detects probable rockfall sources; such regions are defined depending on the distribution of the slope angle derived from crossing very high-resolution DEM with other information obtained from topographic maps and land cover in GIS format. Nevertheless, a major challenge encountered at a regional scale rockfall hazard mapping is the identification of these regions (Loye et al. 2009). Novel remote sensing techniques, such as high-resolution photography and laser scanners, will quantitatively characterize rockfall source regions safely and efficiently (Stock et al. 2011).

15.19.1 Using ALS

Rockfall hazard assessment at a regional scale from source areas to rockfall distribution using ALS–DEM is not regularly implemented. The first challenge is determining rockfall source regions. This step is typically conducted by utilizing the slope angle threshold (Frattini et al. 2008). However, Loye et al. (2009) showed that further details could probably be obtained from slope angle distribution. The threshold depends on the type of bedrock, the DEM resolution, and the absence or presence of a land cover (Loye et al. 2009). This technique allows effectively distinction between a real cliff and one drawn on the topographic map. As proposed by Günther (2003), a structural analysis performed on a DEM acquired via ALS could be the foundation for kinetic tests. Janeras et al. (2004) showed that the result accuracy was significantly enhanced by utilizing a high-resolution DEM.

Rockfall hazard assessment requires frequently executing trajectory modeling for delineating rockfall distribution areas. Rockfall model has been significantly enhanced by using a DEM obtained via ALS (Lan et al. 2007) by offering further dispersal in propagation as indicated by Agliardi and Crosta (2003). Moreover, the profile of kinetic energy is significantly modified with increasing DEM resolution. These parameters are essential for rockfall hazard mapping and for eliminating measurements. Airborne LiDAR was utilized with rockfall spatial modeling by Lan et al. (2010) for a rockfall assessment strategy along a section of a railway. Their group concluded that utilizing LiDAR could explain the usefulness of rockfall hazard assessment along a portion of the railway. ALS allowed them to achieve accurate modeling of terrain geomorphology and to acquire the geometry of significant infrastructure. The simulation results from the high-resolution ALS–DEM present better correspondence with the historic rockfall than the results from coarse DEM. The simulation offers logical rockfall frequency distribution over the railway corridor and the accurate positions of the high possibility of rockfall compared with the historical observations. Topographical analyses utilizing the ALS dataset can also determine possible rockfall source areas based on the slope angle and topographic contrast.

15.19.2 Using TLS

High-resolution DEM is required to implement rockfall simulations and kinematic analyses. In particular, LiDAR techniques are interesting in rockfall hazard assessment because of their capability to produce highly precise and accurate DEMs of the Earth's surface (Barbarella et al. 2013). TLS can provide spatial resolution, high accuracy, and rapid information gathering, and thus, it is becoming increasingly utilized in rockfall research for small areas (Fanti et al. 2013; Gigli et al. 2012; Lato et al. 2012). Gigli et al. (2014) used the TLS technique to provide all the geometric parameters required for implementing rockfall simulations (DEM, main source areas, and the outcropping material limits). Tonini and Abellan (2014) presented a method for extracting features from terrestrial LiDAR point clouds that focused on the recognition of a single rockfall event. The spatial distribution of these events has been analyzed, thereby demonstrating that detected rockfalls are clustered within a well-defined distance ranging from 1 to 3.5 m.

Salvini et al. (2013) and Lato et al. (2013) integrated data from various sources (topographical observations, photogrammetry, and laser scanning) to obtain a DEM of a slope surface, define possible run-out trajectories, and characterize rock mass. They showed that digital terrestrial photogrammetry and TLS provided a powerful analytical tool and model for studying rockfall hazard and the stability of rocky slopes. Gigli et al. (2014) applied TLS in combination with geomechanical surveys at three different areas to cover a wide range of features and examine a proposed approach. TLS was used to structure 3D surface model of the entire slopes to be investigated for kinetic analyses and rockfall modeling and to rebuild the geomechanical characteristics of

the block masses and ultimately identify major rockfall source regions. Each slope was observed from various acquisition points to mitigate the shadow areas as much as possible given slope roughness and scan location limits.

Abellán et al. (2006) used TLS for a comprehensive rockfall research in a test site. High-resolution DEM and the reconstruction of joint geometry were consequently obtained. The DEM was utilized for rockfall inventory and for the accurate simulation of rockfall trajectories and velocities. By contrast, joint geometry enabled modeling of the volume and geometry of the source region in a current rockfall. Their group reported that the TLS technique could be used as a reference tool in rockfall studies in the near future. Janke (2013) compared DEM derivatives (aspect, slope, elevation, curvature, and hillshade) obtained from LiDAR and the US Geological Survey (USGS) DEMs for evaluating rock glaciers. He concluded that the USGS DEMs might suitable for analysis to characterize landform topographical setting at a regional scale. At a fine scale, however, rock glacier topography was illustrated more clearly on the LiDAR DEM, thereby making it a perfect tool for feature acquisition.

15.20 Conclusion

The following conclusions can be drawn from this chapter:

1. Rockfall modeling is frequently implemented via 2D or 3D rockfall model.
2. The selection of a 2D slope profile is crucial to derive practical results of rockfall analysis using 2D models. Such models are restricted in their capability to provide rockfall trajectories spatial distribution, as well as flying or bouncing height and kinetic energy.
3. Several stand-alone 3D rockfall models are accessible for 3D rockfall simulation. These models normally utilize topographic information that are transformed from other information sources, such as geospatial information in regular GRID or TIN, which are typical information constructs in most GIS programs. This information transformation is usually tedious and time-consuming, particularly for a large study area.
4. The accuracy of a DEM is crucial for rockfall assessment. Remote sensing techniques, particularly LiDAR techniques, offer the most accurate DEM among the various techniques for DEM generation.
5. The LiDAR techniques of ALS and TLS are responsible for considerable developments in rock slope characterization. The applications of TLS to characterize rock mass are countless, whereas those of ALS–DEM are still infrequent.
6. Rockfall modeling has two approaches: lumped mass and rigid body. The most popular approach is lumped mass because of its capability to model rockfalls in various motion modes, including flying or free-falling, impacting and rebounding, and rolling or sliding. In addition, the use of rigid body can produce immoderate computational demands that make evaluating rockfall hazard difficult at a regional scale.
7. The identification of rockfall source areas is a challenging task in rockfall simulation.
8. Mechanical parameters significantly affect rockfall trajectories and their characteristics.
9. Numerous studies have been conducted in rockfall hazard assessment. However, most of these studies used specific mechanical parameters but disregarded the uncertainty of these parameters.

References

Abellán, A., Calvet, J., Vilaplana, J. M., & Blanchard, J. (2010). Detection and spatial prediction of rockfalls by means of terrestrial laser scanner monitoring. *Geomorphology, 119*(3), 162–171.

Abellán, A., Jaboyedoff, M., Oppikofer, T., & Vilaplana, J. (2009). Detection of millimetric deformation using a terrestrial laser scanner: Experiment and application to a rockfall event. *Natural Hazards and Earth System Science, 9*(2), 365–372.

Abellán, A., Vilaplana, J., & Martínez, J. (2006). Application of a long-range terrestrial laser scanner to a detailed rockfall study at Vall de Núria (Eastern Pyrenees, Spain). *Engineering Geology, 88*(3), 136–148.

Agliardi, F., & Crosta, G. (2003). High resolution three-dimensional numerical modelling of rockfalls. *International Journal of Rock Mechanics and Mining Sciences, 40*(4), 455–471.

Ahmad, M., Umrao, R., Ansari, M., Singh, R., & Singh, T. (2013). Assessment of rockfall hazard along the road cut slopes of state highway-72, Maharashtra, India. *Geomaterials, 3*(1), 15–23.

Allen, S., & Huggel, C. (2013). Extremely warm temperatures as a potential cause of recent high mountain rockfall. *Global and Planetary Change, 107,* 59–69.

Antoniou, A. A. (2013). GIS-based evaluation of rockfall risk along routes in Greece. *Environmental Earth Sciences, 70*(5), 2305–2318.

Antoniou, A. A., & Lekkas, E. (2010). Rockfall susceptibility map for Athinios port, Santorini island, Greece. *Geomorphology, 118*(1), 152–166.

Antoniou, A., Papadimitriou, A., & Tsiambaos, G. (2008). A geographical information system managing geotechnical data for Athens (Greece) and its use for automated seismic microzonation. *Natural Hazards, 47*(3), 369–395.

Arbanas, Ž., Grošić, M., Udovič, D., & Mihalić, S. (2012). Rockfall hazard analyses and rockfall protection along the Adriatic coast of Croatia. *Journal of Civil Engineering and Architecture, 6*(3), 344–355.

Armesto, J., Ordóñez, C., Alejano, L., & Arias, P. (2009). Terrestrial laser scanning used to determine the geometry of a granite boulder for stability analysis purposes. *Geomorphology, 106*(3), 271–277.

Asteriou, P., Saroglou, H., & Tsiambaos, G. (2012). Geotechnical and kinematic parameters affecting the coefficients of restitution for rock fall analysis. *International Journal of Rock Mechanics and Mining Sciences, 54,* 103–113.

Azzoni, A., La Barbera, G., & Zaninetti, A. (1995). Analysis and prediction of rockfalls using a mathematical model. *International Journal of Rock Mechanics and Mining Sciences & Geomechanics Abstracts*, 709.

Barbarella, M., Fiani, M., & Lugli, A. (2013). Application of LiDAR-derived DEM for detection of mass movements on a landslide. *ISPRS-International Archives of the Photogrammetry, Remote Sensing and Spatial Information Sciences, 1*(3), 89–98.

Basson, F. (2012). Rigid body dynamics for rock fall trajectory simulation. In *46th US Rock Mechanics/Geomechanics Symposium*. American Rock Mechanics Association.

Bater, C. W., & Coops, N. C. (2009). Evaluating error associated with LiDAR-derived DEM interpolation. *Computers & Geosciences, 35*(2), 289–300.

Berry, P., Garlick, J., & Smith, R. (2007). Near-global validation of the SRTM DEM using satellite radar altimetry. *Remote Sensing of Environment, 106*(1), 17–27.

Blahut, J., Klimeš, J., & Vařilová, Z. (2013). Quantitative rockfall hazard and risk analysis in selected municipalities of the České Švýcarsko National Park, Northwestern Czechia. *Geografie, 118*(3), 205–220.

Bornaz, L., Lingua, A., & Rinaudo, F. (2002). Engineering and environmental applications of laser scanner techniques. *International Archives of Photogrammetry Remote Sensing and Spatial Information Sciences, 34*(3/B), 40–43.

Bozzolo, D., & Pamini, R. (1986). Simulation of rock falls down a valley side. *Acta Mechanica, 63*(1–4), 113–130.

Brideau, M., Yan, M., & Stead, D. (2009). The role of tectonic damage and brittle rock fracture in the development of large rock slope failures. *Geomorphology, 103*(1), 30–49.

Buckley, S. J., Howell, J., Enge, H., & Kurz, T. (2008). Terrestrial laser scanning in geology: Data acquisition, processing and accuracy considerations. *Journal of the Geological Society, 165*(3), 625–638.

Bühler, Y., Glover, J., Christen, M., & Bartelt, P. (2014). Digital elevation models in numerical rockfall simulations. In *EGU General Assembly Conference Abstracts* (p. 2109).

Burns, W. J., Coe, J. A., Kaya, B. S., & Ma, L. (2010). Analysis of elevation changes detected from multi-temporal LiDAR surveys in forested landslide terrain in western Oregon. *Environmental and Engineering Geoscience, 16*(4), 315–341.

Carrara, A., Bitelli, G., & Carla, R. (1997). Comparison of techniques for generating digital terrain models from contour lines. *International Journal of Geographical Information Science, 11*(5), 451–473.

Chai, S., Yacoub, T., Charbonneau, K., & Curran, J. (2013). The effect of rigid body impact mechanics on tangential coefficient of restitution. *Geo Montreal*.

Chang, H., Ge, L., Rizos, C., & Milne, T. (2004). Validation of DEMs derived from radar interferometry, airborne laser scanning and photogrammetry by using GPS-RTK. In *Geoscience and Remote Sensing Symposium (IGARSS'04)* (p. 2815). IEEE International.

Chau, K., Wong, R., & Wu, J. (2002). Coefficient of restitution and rotational motions of rockfall impacts. *International Journal of Rock Mechanics and Mining Sciences, 39*(1), 69–77.

Chen, H., Chen, R., & Huang, T. (1994). An application of an analytical model to a slope subject to rockfalls. *Bulletin of the Association of Engineering Geologists, 31*(4), 447–458.

Chiessi, V., D'Orefice, M., Mugnozza, G. S., Vitale, V., & Cannese, C. (2010). Geological, geomechanical and geostatistical assessment of rockfall hazard in San Quirico Village (Abruzzo, Italy). *Geomorphology, 119*(3), 147–161.

Crosta, G., & Agliardi, F. (2004). Parametric evaluation of 3D dispersion of rockfall trajectories. *Natural Hazards and Earth System Science, 4*(4), 583–598.

Day, R. W. (1997). Case studies of rockfall in soft versus hard rock. *Environmental and Engineering Geoscience, 3*(1), 133–140.

Dorren, L. K. (2003). A review of rockfall mechanics and modelling approaches. *Progress in Physical Geography, 27*(1), 69–87.

Dorren, L. K., & Seijmonsbergen, A. C. (2003). Comparison of three GIS-based models for predicting rockfall runout zones at a regional scale. *Geomorphology, 56*(1), 49–64.

Douglas, G. (1980). Magnitude frequency study of rockfall in Co., Antrim, N. Ireland. *Earth Surface Processes, 5*(2), 123–129.

Dussauge-Peisser, C., Helmstetter, A., Grasso, J., Hantz, D., Desvarreux, P., Jeannin, M., et al. (2002). Probabilistic approach to rock fall hazard assessment: Potential of historical data analysis. *Natural Hazards and Earth System Science, 2*(1/2), 15–26.

Erismann, T. (1986). Flowing, rolling, bouncing, sliding: Synopsis of basic mechanisms. *Acta Mechanica, 64*(1–2), 101–110.

Evans, S., & Hungr, O. (1993). The assessment of rockfall hazard at the base of talus slopes. *Canadian Geotechnical Journal, 30*(4), 620–636.

Fanti, R., Gigli, G., Lombardi, L., Tapete, D., & Canuti, P. (2013). Terrestrial laser scanning for rockfall stability analysis in the cultural heritage site of Pitigliano (Italy). *Landslides, 10*(4), 409–420.

Fanos, A.M., & Pradhan, B. (2016). Multi-scenario Rockfall Hazard Assessment Using LiDAR Data and GIS. *Geotechnical and Geological Engineering*, *34*(5), 1375–1393. http://dx.doi.org/10.1007/s10706-016-0049-z.

Fanos, A.M., Pradhan, B., Aziz, A.A., Jebur, M.N., & Park, H. J. (2016). Assessment of multi-scenario rockfall hazard based on mechanical parameters using high-resolution airborne laser scanning data and GIS in a tropical area. *Environmental Earth Sciences*, *75*, 1129. http://dx.doi.org/1007/s12665-016-5936-3.

Feng, Q., Sjögren, P., Stephansson, O., & Jing, L. (2001). Measuring fracture orientation at exposed rock faces by using a non-reflector total station. *Engineering Geology, 59*(1), 133–146.

Ferrari, F., Giani, G. P., & Apuani, T. (2013). Why can rockfall normal restitution coefficient be higher than one? *Rendiconti online Società Geologica Italiana*, 122.

Firpo, G., Salvini, R., Francioni, M., & Ranjith, P. (2011). Use of digital terrestrial photogrammetry in rocky slope stability analysis by distinct elements numerical methods. *International Journal of Rock Mechanics and Mining Sciences, 48*(7), 1045–1054.

Fish, M., & Lane, R. (2002). Linking New Hampshire's rock cut management system with a geographic information system. *Transportation Research Record: Journal of the Transportation Research Board, no., 1786,* 51–59.

Florinsky, I. V. (1998). Accuracy of local topographic variables derived from digital elevation models. *International Journal of Geographical Information Science, 12*(1), 47–62.

Frattini, P., Crosta, G. B., Agliardi, F., & Imposimato, S. (2013). Challenging calibration in 3D rockfall modelling. In *Landslide science and practice* (pp. 169–175). Berlin: Springer.

Frattini, P., Crosta, G., Carrara, A., & Agliardi, F. (2008). Assessment of rockfall susceptibility by integrating statistical and physically-based approaches. *Geomorphology, 94*(3), 419–437.

Fritz, A., Kattenborn, T., & Koch, B. (2013). UAV-based photogrammetric point clouds-tree stem mapping in open stands in comparison to terrestrial laser scanner point clouds. *International Archives of the Photogrammetry, Remote Sensing and Spatial Information Sciences, XL, 1,* W2.

Froese, C. R., Moreno, F., Jaboyedoff, M., & Cruden, D. M. (2009). 25 years of movement monitoring on South Peak, Turtle Mountain: Understanding the hazard. *Canadian Geotechnical Journal, 46*(3), 256–269.

Gallay, M., Lloyd, C. D., McKinley, J., & Barry, L. (2013). Assessing modern ground survey methods and airborne laser scanning for

digital terrain modelling: A case study from the Lake District, England. *Computers & Geosciences, 51,* 216–227.

Gardner, J. (1983). Rockfall frequency and distribution in the Highwood Pass area, Canadian Rocky Mountains. *Zeitschrift für Geomorphologie, 27*(3), 311–324.

Gigli, G., Frodella, W., Mugnai, F., Tapete, D., Cigna, F., Fanti, R., et al. (2012). Instability mechanisms affecting cultural heritage sites in the Maltese Archipelago. *Natural Hazards and Earth System Sciences, 12,* 1883–1903.

Gigli, G., Morelli, S., Fornera, S., & Casagli, N. (2014). Terrestrial laser scanner and geomechanical surveys for the rapid evaluation of rock fall susceptibility scenarios. *Landslides, 11*(1), 1–14.

Giordan, D., Manconi, A., Facello, A., Baldo, M., Allasia, P., & Dutto, F. (2014). "Brief communication" the use of UAV in rock fall emergency scenario. *Natural Hazards and Earth System Sciences Discussions, 2*(6), 4011–4029.

Glover, J., Bartelt, P., Christen, M., & Gerber, W. (2015). Rockfall-simulation with irregular rock blocks. In *Engineering geology for society and territory* (Vol. 2, pp. 1729–1733). Berlin: Springer.

Günther, A. (2003). SLOPEMAP: Programs for automated mapping of geometrical and kinematical properties of hard rock hill slopes. *Computers & Geosciences, 29*(7), 865–875.

Guzzetti, F., Crosta, G., Detti, R., & Agliardi, F. (2002). STONE: A computer program for the three-dimensional simulation of rock-falls. *Computers & Geosciences, 28*(9), 1079–1093.

Haarbrink, R., & Eisenbeiss, H. (2008). Accurate DSM production from unmanned helicopter systems. *The International Archives of the Photogr ammetry, Remote Sensing and Spatial Information Sciences., 37,* 1259–1264.

Haneberg, W. C. (2007). Directional roughness profiles from three-dimensional photogrammetric or laser scanner point clouds. In E. Eberhardt, D. Stead, & T. Morrison (Eds.), *Rock mechanics: Meeting society's challenges and demands* (p. 101).

Hegg, C., & Kienholz, H. (1995). Determining paths of gravity-driven slope processes: The 'vector tree model'. In *Geographical information systems in assessing natural hazards* (pp. 79–92). Berlin: Springer.

Hengl, T., Heuvelink, G., & Van Loon, E. (2010). On the uncertainty of stream networks derived from elevation data: The error propagation approach. *Hydrology and Earth System Sciences, 14*(7), 1153–1165.

Hétu, B., & Gray, J. T. (2000). Effects of environmental change on scree slope development throughout the postglacial period in the Chic-Choc Mountains in the northern Gaspé Peninsula, Québec. *Geomorphology, 32*(3), 335–355.

Höfle, B., & Rutzinger, M. (2011). Topographic airborne LiDAR in geomorphology: A technological perspective. *Zeitschrift für Geomorphologie, Supplementary Issues, 55*(2), 1–29.

Hofton, M., Dubayah, R., Blair, J. B., & Rabine, D. (2006). Validation of SRTM elevations over vegetated and non-vegetated terrain using medium footprint lidar. *Photogrammetric Engineering & Remote Sensing, 72*(3), 279–285.

Hungr, O., & Evans, S. (1988). Engineering evaluation of fragmental rockfall hazards. In *Proceedings of the Fifth International Symposium on Landslides, Lausanne, AA Balkema, Rotterdam, Netherlands* (p. 685).

Hutchinson, M. F., & Gallant, J. C. (2000). Digital elevation models and representation of terrain shape. In *Terrain analysis: Principles and applications* (pp. 29–50).

Jaboyedoff, M., Choffet, M., Derron, M., Horton, P., Loye, A. Longchamp, C., et al. (2012a). Preliminary slope mass movement susceptibility mapping using DEM and LiDAR DEM. In *Terrigenous mass movements* (pp. 109–170). Berlin: Springer.

Jaboyedoff, M., & Labiouse, V. (2011). Technical Note: Preliminary estimation of rockfall runout zones. *Natural Hazards and Earth System Science, 11*(3), 819–828.

Jaboyedoff, M., Oppikofer, T., Abellán, A., Derron, M., Loye, A., Metzger, R., et al. (2012b). Use of LIDAR in landslide investigations: A review. *Natural Hazards, 61*(1), 5–28.

Jaboyedoff, M., Oppikofer, T., Locat, A., Locat, J., Turmel, D., Robitaille, D., et al. (2009b). Use of ground-based LIDAR for the analysis of retrogressive landslides in sensitive clay and of rotational landslides in river banks. *Canadian Geotechnical Journal, 46,* 1379–1390.

James, L. A., Watson, D. G., & Hansen, W. F. (2007). Using LiDAR data to map gullies and headwater streams under forest canopy: South Carolina, USA. *Catena, 71*(1), 132–144.

Janeras, M., Navarro, M., Arnó, G., Ruiz, A., Kornus, W., Talaya, J., et al. (2004). LiDAR applications to rock fall hazard assesment in Vall de Núria. In *4th ICA Mountain Cartography Workshop, Vall de Núria, Catalonia, Spain* (p. 1).

Janke, J. R. (2013). Using airborne LiDAR and USGS DEM data for assessing rock glaciers and glaciers. *Geomorphology, 195,* 118–130.

Jomelli, V., & Francou, B. (2000). Comparing the characteristics of rockfall talus and snow avalanche landforms in an Alpine environment using a new methodological approach: Massif des Ecrins, French Alps. *Geomorphology, 35*(3), 181–192.

Kemeny, J., & Post, R. (2003). Estimating three-dimensional rock discontinuity orientation from digital images of fracture traces. *Computers & Geosciences, 29*(1), 65–77.

Keskin, İ. (2013). Evaluation of rock falls in an urban area: The case of Boğaziçi (Erzincan/Turkey). *Environmental Earth Sciences, 70*(4), 1619–1628.

Keylock, C., & Domaas, U. (1999). Evaluation of topographic models of rockfall travel distance for use in hazard applications. *Arctic, Antarctic, and Alpine Research, 31*(3), 312–320.

Kirkby, M., & Statham, I. (1975). Surface stone movement and scree formation. *The Journal of Geology, 83*(3), 349–362.

Ku, C. (2012). Assessing rockfall hazards using a three-dimensional numerical model based on high resolution DEM. In *The Twenty-second International Offshore and Polar Engineering ConferenceInternational Society of Offshore and Polar Engineers* (p. 790).

Lan, H. Derek, Martin, C., & Lim, C. (2007). RockFall analyst: A GIS extension for three-dimensional and spatially distributed rockfall hazard modeling. *Computers & Geosciences, 33*(2), 262–279.

Lan, H., Martin, C. D., Zhou, C., & Lim, C. H. (2010). Rockfall hazard analysis using LiDAR and spatial modeling. *Geomorphology, 118* (1), 213–223.

Lato, M., Diederichs, M. S., Hutchinson, D. J., & Harrap, R. (2009a). Optimization of LiDAR scanning and processing for automated structural evaluation of discontinuities in rockmasses. *International Journal of Rock Mechanics and Mining Sciences, 46*(1), 194–199.

Lato, M. J., Diederichs, M. S., Hutchinson, D. J., & Harrap, R. (2012). Evaluating roadside rockmasses for rockfall hazards using LiDAR data: Optimizing data collection and processing protocols. *Natural Hazards, 60*(3), 831–864.

Lato, M., Hutchinson, J., Diederichs, M., Ball, D., & Harrap, R. (2009b). Engineering monitoring of rockfall hazards along transportation corridors: Using mobile terrestrial LiDAR. *Natural Hazards and Earth System Sciences, 9*(3), 935–946.

Lato, M., Kemeny, J., Harrap, R., & Bevan, G. (2013). Rock bench: Establishing a common repository and standards for assessing rockmass characteristics using LiDAR and photogrammetry. *Computers & Geosciences, 50,* 106–114.

Lee, K., & Elliott, G. (1998). *Rockfall: Application of computer simulation to design of preventive measures, planning, design and*

implementation of debris flow and rockfall hazards mitigation measures (pp. 47–65). Hong Kong: Association of Geo-Technical Specialists & Hong Kong Institution of Engineers.

Leine, R., Schweizer, A., Christen, M., Glover, J., Bartelt, P., & Gerber, W. (2013). Simulation of rockfall trajectories with consideration of rock shape. *Multibody System Dynamics, 32*(2), 1–31.

Li, L., & Lan, H. (2015). Probabilistic modeling of rockfall trajectories: A review. *Bulletin of Engineering Geology and the Environment, 74* (4), 1163–1176.

Lopez-Saez, J., Corona, C., Eckert, N., Stoffel, M., Bourrier, F., & Berger, F. (2016). Impacts of land-use and land-cover changes on rockfall propagation: Insights from the Grenoble conurbation. *Science of the Total Environment, 547,* 345–355.

Loye, A., Jaboyedoff, M., & Pedrazzini, A. (2009). Identification of potential rockfall source areas at a regional scale using a DEM-based geomorphometric analysis. *Natural Hazards and Earth System Science, 9*(5), 1643–1653.

Luckman, B. (1976). Rockfalls and rockfall inventory data: Some observations from Surprise Valley, Jasper National Park, Canada. *Earth Surface Processes, 1*(3), 287–298.

Ma, G., Matsuyama, H., Nishiyama, S., & Ohnishi, Y. (2011). Practical studies on rockfall simulation by DDA. *Journal of Rock Mechanics and Geotechnical Engineering, 3*(1), 57–63.

Macciotta, R., Cruden, D., Martin, C., & Morgenstern, N. (2011). Combining geology, morphology and 3D modelling to understand the rock fall distribution along the railways in the Fraser River Valley, between Hope and Boston Bar. In *BC International Symposium on Rock Slope Stability in Open Pit Mining and Civil Engineering, Vancouver, BC, Canada*.

Macciotta, R., Martin, C. D., & Cruden, D. M. (2014). Probabilistic estimation of rockfall height and kinetic energy based on a three-dimensional trajectory model and Monte Carlo simulation. *Landslides, 12*(4), 1–16.

Martin, D. C. (1988). Rockfall control: An update (technical note). *Bulletin Association Engineering Geologists, 13*(14), 329–335.

Masuya, H., Amanuma, K., Nishikawa, Y., & Tsuji, T. (2009). Basic rockfall simulation with consideration of vegetation and application to protection measure. *Natural Hazards and Earth System Science, 9*(6), 1835–1843.

Michoud, C., Derron, M., Horton, P., Jaboyedoff, M., Baillifard, F., Loye, A., et al. (2012). Rockfall hazard and risk assessments along roads at a regional scale: Example in Swiss Alps. *Natural Hazards and Earth System Sciences, 12*(3), 615–629.

Mikoš, M., Petje, U., & Ribičič, M. (2006). *Application of a rockfall simulation program in an alpine valley in Slovenia* (pp. 199–211). Slopes, Failures and Landslides: Disaster Mitigation of Debris Flows.

Monserrat, O., & Crosetto, M. (2008). Deformation measurement using terrestrial laser scanning data and least squares 3D surface matching. *ISPRS Journal of Photogrammetry and Remote Sensing, 63*(1), 142–154.

Nelson, A., Reuter, H. I., & Gessler, P. (2009). Chapter 3 DEM production methods and sources. *Developments in Soil Science*, *33*, 65–85.

Niethammer, U., James, M., Rothmund, S., Travelletti, J., & Joswig, M. (2012). UAV-based remote sensing of the Super-Sauze landslide: Evaluation and results. *Engineering Geology, 128,* 2–11.

Niethammer, U., Rothmund, S., James, M., Travelletti, J., & Joswig, M. (2010). UAV-based remote sensing of landslides. *International Archives of Photogrammetry, Remote Sensing and Spatial Information Sciences, 38*(Part 5), 496–501.

Olaya, V. (2009). Chapter 6 basic land-surface parameters. *Developments in Soil Science, 33*, 141–169.

Oppikofer, T., Jaboyedoff, M., Blikra, L., Derron, M., & Metzger, R. (2009). Characterization and monitoring of the Åknes rockslide using terrestrial laser scanning. *Natural Hazards and Earth System Science, 9*(3), 1003–1019.

Oppikofer, T., Jaboyedoff, M., & Keusen, H. (2008). Collapse at the eastern Eiger flank in the Swiss Alps. *Nature Geoscience, 1*(8), 531–535.

Papathanassiou, G., Marinos, V., Vogiatzis, D., & Valkaniotis, S. (2013). A rock fall analysis study in Parnassos area, Central Greece. In *Landslide science and practice* (pp. 67–72). Berlin: Springer.

Pfeiffer, T. J., & Bowen, T. (1989). Computer simulation of rockfalls. *Bulletin of the Association of Engineering Geologists, 26*(1), 135–146.

Pradhan, B., & Lee, S. (2010). Regional landslide susceptibility analysis using back-propagation neural network model at Cameron Highland, Malaysia. *Landslides, 7*(1), 13–30.

Pradhan, B., Mansor, S., Pirasteh, S., & Buchroithner, M. F. (2011). Landslide hazard and risk analyses at a landslide prone catchment area using statistical based geospatial model. *International Journal of Remote Sensing, 32*(14), 4075–4087.

Pradhan, B., Mansor, S., Ramli, A. R., Mohamed Sharif, A. R. B., & Sandeep, K. (2005). LiDAR data compression using wavelets. *Remote Sensing International Society for Optics and Photonics*, 598305.

Pradhan, B., OHb, H., & Buchroithner, M. (2010). Use of remote sensing data and GIS to produce a landslide susceptibility map of a landslide prone area using a weight of evidence model. *Assessment, 11*, 13.

Raaflaub, L. D., & Collins, M. J. (2006). The effect of error in gridded digital elevation models on the estimation of topographic parameters. *Environmental Modelling and Software, 21*(5), 710–732.

Rayburg, S., Thoms, M., & Neave, M. (2009). A comparison of digital elevation models generated from different data sources. *Geomorphology, 106*(3), 261–270.

Reuter, H. I., Hengl, T., Gessler, P., & Soille, P. (2009). Chapter 4 Preparation of DEMs for geomorphometric analysis, *Developments in Soil Science, 33*, 87–120.

Richards, L. (1988). Rockfall protection: A review of current analytical and design methods. *Secondo ciclo di conferenze di meccanica ed ingegneria delle rocce, MIR, Politecnico di Torino, 11,* 1–13.

Ritchie, A. M. (1963). Evaluation of rockfall and its control. *Highway research record, no., 17,* 13–28.

Rodriguez, E., Morris, C. S., & Belz, J. E. (2006). A global assessment of the SRTM performance. *Photogrammetric Engineering & Remote Sensing, 72*(3), 249–260.

Rosser, N., Lim, M., Petley, D., Dunning, S., & Allison, R. (2007). Patterns of precursory rockfall prior to slope failure. *Journal of Geophysical Research: Earth Surface (2003–2012), 112*(F4), 1–14.

Ruff, M., & Czurda, K. (2008). Landslide susceptibility analysis with a heuristic approach in the Eastern Alps (Vorarlberg, Austria). *Geomorphology, 94*(3), 314–324.

Ruiz, J., Diaz-Mas, L., Perez, F., & Viguria, A. (2013). Evaluating the accuracy of DEM generation algorithms from UAV imagery. *International Archives of the Photogrammetry, Remote Sensing and Spatial Information Sciences, 40,* 333–337.

Sabatakakis, N., Depountis, N., & Vagenas, N. (2015). Evaluation of rockfall restitution coefficients. In *Engineering geology for society and territory* (Vol. 2, pp. 2023–2026). Berlin: Springer.

Salvini, R., Francioni, M., Riccucci, S., Bonciani, F., & Callegari, I. (2013). Photogrammetry and laser scanning for analyzing slope stability and rock fall runout along the Domodossola-Iselle railway, the Italian Alps. *Geomorphology, 185,* 110–122.

Samodra, G., Chen, G., Sartohadi, J., Hadmoko, D., & Kasama, K. (2014). Automated landform classification in a rockfall-prone area, Gunung Kelir, Java. *Earth Surface Dynamics, 2*(1), 339–348.

Samodra, G., Sartohadi, J., Chen, G., & Kasama, K. (2013). *Application of supervised landform classification of 9-unit slope*

model for preliminary rockfall risk analysis in Gunung Kelir, Java (pp. O-8-1–O-8-4), Geo morphometry.org.

Shary, P. A., Sharaya, L. S., & Mitusov, A. V. (2002). Fundamental quantitative methods of land surface analysis. *Geoderma, 107*(1), 1–32.

Slob, S., Hack, H., & Turner, A. K. (2002). An approach to automate discontinuity measurements of rock faces using laser scanning techniques. *Proceedings of ISRM EUROCK, 2002,* 87–94.

Spadari, M., Kardani, M. De, Carteret, R., Giacomini, A., Buzzi, O., Fityus, S., et al. (2013). Statistical evaluation of rockfall energy ranges for different geological settings of New South Wales, Australia. *Engineering Geology, 158,* 57–65.

Spang, R., & Rautenstrauch, R. (1988). Empirical and mathematical approaches to rockfall protection and their practical applications. In *5th International Symposium on Landslides* (p. 1237).

Statham, I., & Francis, S. (1986). *Influence of scree accumulation and weathering on the development of steep mountain slopes* (pp. 245–267). Hillslope Processes. (Abrahams AD).

Stephenne, N., Frippiat, C., Veschkens, M., Salmon, M., & Pacyna, D. (2014). Use of a LiDAR high resolution digital elevation model for risk stability analysis. *EARSeL eProceedings, 13*(S1), 24–29.

Stock, G. M., Bawden, G. W., Green, J. K., Hanson, E., Downing, G., Collins, B. D., et al. (2011). High-resolution three-dimensional imaging and analysis of rock falls in Yosemite Valley, California. *Geosphere, 7*(2), 573–581.

Strozzi, T., Delaloye, R., Kääb, A., Ambrosi, C., Perruchoud, E., & Wegmüller, U. (2010). Combined observations of rock mass movements using satellite SAR interferometry, differential GPS, airborne digital photogrammetry, and airborne photography interpretation. *Journal of Geophysical Research: Earth Surface (2003–2012), 115*(F1).

Sturzenegger, M., & Stead, D. (2009). Quantifying discontinuity orientation and persistence on high mountain rock slopes and large landslides using terrestrial remote sensing techniques. *Natural Hazards and Earth System Science, 9*(2), 267–287.

Sturzenegger, M., Yan, M., Stead, D., & Elmo, D. (2007). Application and limitations of ground-based laser scanning in rock slope characterization. In *Proceedings of the First Canadian US Rock Mechanics Symposium* (p. 29).

Tatone, B. S., & Grasselli, G. (2009). A method to evaluate the three-dimensional roughness of fracture surfaces in brittle geomaterials. *Review of Scientific Instruments, 80*(12), 125110.

Temme, A. J. A. M., Heuvelink, G. B. M., Schoorl, J. M., & Claessens, L. (2009). Chapter 5 geostatistical simulation and error propagation in geomorphometry. *Developments in Soil Science, 33*, 121–140.

Tonini, M., & Abellan, A. (2014). "Rockfall detection from terrestrial LiDAR point clouds: A clustering approach using R", Journal of Spatial Information Science, no. *To appear JOSIS issue, 8,* 95–101.

Topal, T., Akin, M., & Ozden, U. A. (2007). Assessment of rockfall hazard around Afyon Castle, Turkey. *Environmental Geology, 53* (1), 191–200.

Varnes, D. J. (1978). Slope movement types and processes. *Transportation Research Board Special Report, no., 176,* 11–33.

Varnes, D. J. (1984). *Landslide hazard zonation: A review of principles and practice* (p. 64).

Vidrih, R., Ribičič, M., & Suhadolc, P. (2001). Seismogeological effects on rocks during the 12 April 1998 upper Soča Territory earthquake (NW Slovenia). *Tectonophysics, 330*(3), 153–175.

Vijayakumar, S., Yacoub, T., & Curran, J. H. (2011). *On the effect of rock size and shape in rockfall analyses*. USA: Proceedings of the US Rock Mechanics Symposium (ARMA) San Francisco CA.

Vijayakumar, S., Yacoub, T., Ranjram, M., & Curran, J. (2012). Effect of rockfall shape on normal coefficient of restitution. In *46th US Rock Mechanics/Geomechanics Symposium*. American Rock Mechanics Association.

Volkwein, A., Schellenberg, K., Labiouse, V., Agliardi, F., Berger, F., Bourrier, F., et al. (2011). Rockfall characterisation and structural protection-a review. *Natural Hazards and Earth System Sciences, 11,* 2617–2651.

Wang, I., & Lee, C. (2012). Simulation and statistical analysis of motion behavior of a single rockfall. *International Journal of Civil and Environmental Engineering, 61,* 853–862.

Webster, T. L., & Dias, G. (2006). An automated GIS procedure for comparing GPS and proximal LiDAR elevations. *Computers & Geosciences, 32*(6), 713–726.

Wieczorek, G. F., Snyder, J. B., Waitt, R. B., Morrissey, M. M., Uhrhammer, R. A., Harp, E. L., et al. (2000). Unusual July 10, 1996, rock fall at Happy Isles, Yosemite National Park, California. *Geological Society of America Bulletin, 112*(1), 75–85.

Wilson, J. P. (2012). Digital terrain modeling. *Geomorphology, 137*(1), 107–121.

Wilson, J. P., Aggett, G., & Yongxin, D. (2008). Water in the landscape: A review of contemporary flow routing algorithms. In *Advances in digital terrain analysis* (pp. 213–236). Berlin: Springer.

Wilson, J. P., & Burrough, P. A. (1999). Dynamic modeling, geostatistics, and fuzzy classificaiton: New sneakers for a new geography? *Annals of the Association of American Geographers, 89* (4), 736–746.

Wise, S. (2000). Assessing the quality for hydrological applications of digital elevation models derived from contours. *Hydrological Processes, 14*(11–12), 1909–1929.

Wise, S. (2011). Cross-validation as a means of investigating DEM interpolation error. *Computers & Geosciences, 37*(8), 978–991.

Wyllie, D. C. (2014). Calibration of rock fall modeling parameters. *International Journal of Rock Mechanics and Mining Sciences, 67,* 170–180.

Yoshimatsu, H., & Abe, S. (2006). A review of landslide hazards in Japan and assessment of their susceptibility using an analytical hierarchic process (AHP) method. *Landslides, 3*(2), 149–158.

Youssef, A. M., Pradhan, B., Al-Kathery, M., Bathrellos, G. D., & Skilodimou, H. D. (2015). Assessment of rockfall hazard at Al-Noor Mountain, Makkah city (Saudi Arabia) using spatio-temporal remote sensing data and field investigation. *Journal of African Earth Sciences, 101,* 309–321.

Zandbergen, P. (2008). Applications of shuttle radar topography mission elevation data. *Geography Compass, 2*(5), 1404–1431.

Zinggeler, A., Krummenacher, B., & Kienholz, H. (1991). Steinschlagsimulation in Gebirgswäldern. *Berichte und Forschungen, 3,* 61–70.